

Probing the Chaos to Integrability Transition in Double-Scaled SYK

Sergio E. Aguilar-Gutierrez ,^a **Rathindra Nath Das** ,^{b,c,d} **Johanna Erdmenger** ,^b and **Zhuo-Yu Xian** ,^e

^a *Qubits and Spacetime Unit, Okinawa Institute of Science and Technology Graduate University,¹ Onna, Okinawa 904 0495, Japan*

^b *Institute for Theoretical Physics and Astrophysics and Würzburg-Dresden Cluster of Excellence ctd.qmat, Julius-Maximilians-Universität Würzburg, Am Hubland, 97074 Würzburg, Germany*

^c *Department of Particle Physics and Astrophysics, Weizmann Institute of Science, Rehovot 7610001, Israel*

^d *MIT Center for Theoretical Physics—a Leinweber Institute, Massachusetts Institute of Technology, 77 Massachusetts Ave., Cambridge, MA 02139*

^e *Department of Physics, Freie Universität Berlin, Arnimallee 14, DE-14195 Berlin, Germany*

E-mail: sergio.ernesto.aguilar@gmail.com,

das.rathindranath@uni-wuerzburg.de,

johanna.erdmenger@uni-wuerzburg.de, zhuo-yu.xian@fu-berlin.de

ABSTRACT: We investigate how a thermodynamical first-order phase transition affects the dynamical chaotic behaviour of a given model. To this effect, we analyze the model of Berkooz, Brukner, Jia and Mamroud that interpolates between the double-scaled SYK model and an integrable chord Hamiltonian. This model displays a first-order phase transition given by a kink in the free energy. We map out the dynamical behaviour, as characterized by chord number, Krylov complexity, and operator size, of the model across the phase diagram. We observe a jump in the chord numbers at the transition point, in agreement with the first-order transition. We further determine how scrambling measures, i.e. the growth of the Lanczos coefficients and the time dependence of the operator size, change across the phase diagram. Deep inside the two phases, these measures indeed display integrable and chaotic behaviour, respectively. Across the transition however, we observe no qualitative change in these measures. This means that the thermodynamical transition does not imply a sharp transition in the growth exponent characterizing the dynamical chaotic behaviour. We also discuss a possible holographic interpretation of the model.

¹ 沖縄科学技術大学学院大学

Contents

| | | |
|----------|---|-----------|
| 1 | Introduction | 2 |
| 2 | The integrable-chaotic model and its phase transition | 5 |
| 2.1 | The BBJM model and its chord Hilbert space | 5 |
| 2.2 | Effective action and phase transition | 7 |
| 2.3 | Evolution of chord numbers | 9 |
| 3 | Discussion on the Krylov basis | 12 |
| 3.1 | General Krylov basis | 12 |
| 3.2 | Special case: $q_{nn} = q_{nz} = q_{zz}$ | 13 |
| 4 | Krylov operator complexity across the phase transition | 14 |
| 4.1 | Krylov operator complexity | 14 |
| 4.2 | Perturbative approach to Krylov operator complexity | 16 |
| 5 | Operator size growth across the phase transition | 18 |
| 6 | Discussion | 21 |
| 6.1 | Outlook | 22 |
| A | Supplementary Background Material | 25 |
| A.1 | Krylov state (spread) complexity | 25 |
| A.2 | Krylov operator complexity | 26 |
| A.3 | OTOCs at finite temperature | 27 |
| A.4 | The Double-Scaled SYK and Commuting SYK Models | 29 |
| A.5 | Multifield Liouville formulation | 30 |
| B | More details about (2.8) | 31 |
| C | Deviations from the $q_{nn} = q_{nz} = q_{zz}$ Krylov basis | 31 |

1 Introduction

Phase transitions play a central role in understanding how many-body systems reorganize under changes in thermodynamic control parameters, and it is natural to ask how signatures of quantum chaos behave across such transitions. There has been considerable interest in exploring various measures of quantum chaos including early-time measures such as out-of-time-ordered correlators (OTOCs)[1, 2], and late-time measures such as the spectral form factor [3]; level spacing spectral statistics [4–6]; Krylov complexity for operators [7] and states [8, 9]; see [10–12] for reviews. In particular, several works have found that Krylov complexity is a useful measure to characterize systems transitioning between chaotic and integrable properties [13–20].

In this work we consider the model of Berkooz, Brukner, Jia and Mamroud (BBJM) [21, 22] as a concrete framework to study a phase transition between integrable and chaotic behaviour (see also [23, 24]). In its simplest version, the BBJM model is built from two decoupled Hamiltonians in a double-scaling limit,¹ in which each theory can be described by the techniques of chord diagrams, namely

$$\hat{H} = \nu \hat{H}_1 + \kappa \hat{H}_2, \quad |\nu|^2 + |\kappa|^2 = 1. \quad (1.1)$$

We take \hat{H}_1 to be the chord Hamiltonian of the double-scaled SYK (DSSYK) model [26, 27], reviewed in [28];² where maximal chaos in terms of fake temperature [37] is well-established in terms of different chaos measures [38–40]. Meanwhile \hat{H}_2 is an integrable chord Hamiltonian [21], where one may consider a commuting SYK model [41] in the double-scaling regime [21, 22, 24, 25], or an integrable spin chain.³ Here, we allow crossings between both integrable and chaotic Hamiltonian chords, although there is no coupling between the chaotic/integrable Hamiltonians.

Despite the remarkable progress in understanding the properties of this model, chaos and integrability in the first and second-order phase transitions are, arguably, not well-understood. Following the terminology of BBJM [21, 22], we will refer to the phase continuously connected to the purely chaotic system with $\kappa = 0$ as the *chaotic phase*, and to the phase continuously connected to the purely integrable system with $\nu = 0$ as the *quasi-integrable phase*.

While there is a clear distinction between the two phases on both sides of the transition point as captured by the free energy; it is unknown whether this thermodynamic distinction is reflected in dynamical measures of quantum chaos [21, 22]. Specifically, it is not clear whether the phase dominated by the commuting chord Hamiltonian displays the characteristic signatures of integrability in dynamical probes—such as polynomial growth of Krylov complexity and operator size, or the absence of exponential Lyapunov growth in OTOCs—or whether

¹This can be extended by including chords with “flavours” [23, 25].

²Quantum groups and von Neumann algebras in this and other closely related systems have been explored in [27, 29–36].

³A more general formalism with an arbitrary number of chord Hamiltonians was later developed in [23, 25], which we review in App. A.5.

the phase dominated by the DSSYK sector robustly exhibits chaotic features such as linearly growing Lanczos coefficients and exponential size/OTOC growth throughout its parameter range, especially near the transition. Moreover, it is a priori unclear whether these standard chaos diagnostics themselves undergo a sharp change at the first-order transition, or instead only interpolate smoothly even when the free energy has a kink. This is an important feature to understand if the model could be realized in a table-top experiment (e.g. [42]), such as those that motivated the previous investigation by [21, 22].

In addition, recent developments indicate that the holographic dual of the DSSYK model and the commuting DSSYK are sine dilaton gravity [30, 43, 43–49] and its flat space limit [44] respectively.⁴ Krylov complexity is a central entry in the holographic dictionary of the DSSYK model. It has a geometric realization as a wormhole length in the dual bulk theory [35, 37, 38, 40, 73, 76–80]. It is important to develop this program further, in particular in view of understanding the consequences of the integrable deformations in the DSSYK for the holographic dictionary beyond standard the anti-de Sitter (AdS)/conformal field theory (CFT) correspondence.

Although the BBJM model (1.1) exhibits integrable and chaotic phases far from the transition point, near the transition line the distinction between integrable or chaotic behaviour - as quantified by measures of quantum chaos - is less obvious. A first order phase transition does not necessarily lead to a dramatic change in chaotic properties. For example, charged black holes may undergo a first order phase transition between the large black hole phase and small black hole phase [81, 82], but both of them saturate Lyapunov exponent bounds [83, 84].

In order to further characterize the behaviour across the phase transition, we consider scrambling, i.e. how local information spreads across the system, rather than spectral statistics as characterized by the spectral form factor. Level-spacing statistics characterizes quantum chaos through random matrix behaviour of energy levels. These measures are well defined for systems with a discrete energy spectrum, such as a single realization of the SYK model and the commuting SYK. However, we work with an auxiliary system describing ensemble-averaged observables of the physical SYK [85, 86] and the commuting SYK [41] models in the strict $N \rightarrow \infty$ limit, where N denotes the total number of degrees of freedom. Spectral measures of chaos are not well-defined for systems with a continuous energy spectrum,⁵ which is the case in our study. For this reason, we will quantify scrambling through appropriate

⁴Other proposals for the holographic dual to the DSSYK model include three-dimensional de Sitter (dS₃) space [48, 50–55], and dS₂ Jackiw-Teitelboim (JT) gravity [56, 57] as a dimensional reduction of dS₃ space [58–68], among others [55, 69–72]. These proposals may be related among each other, and including sine dilaton gravity [48, 73–76].

⁵In terms of standard AdS/CFT, we consider early-time chaotic measures (OTOCs and Krylov complexity) capturing $N \rightarrow \infty$ limit in the boundary theory, corresponding to the disk topology in the Euclidean path integral in the bulk dual. In contrast, to capture the ramp-plateau behavior of the spectral form factor predicted by random matrix theory, as well as the saturation value of Krylov complexity, at sufficiently late times, one needs to include perturbative and non-perturbative effects of finite N in the boundary theory, corresponding to wormhole and higher genus topologies in the bulk.

diagnostics, such as Krylov complexity and OTOCs. This leads us to address the question

Do the quasi-integrable and chaotic phases that are separated by the first order phase transition show different signatures of scrambling?

In this work we answer this question by examining the integrable-chaotic chord Hamiltonian model proposed in [21, 22] using different measures of quantum chaos. We focus on (i) deriving the Krylov basis for spread complexity with the thermo-field double (TFD) as the reference state in the Lanczos algorithm, (ii) Krylov operator complexity and (iii) OTOCs at finite temperature for integrable and chaotic matter chord operators. The purpose of these diagnostics is to test whether the quasi-integrable and chaotic phases display the expected scrambling behaviour of integrable or chaotic systems.⁶ Deep inside the two phases, the chaos measures behave very differently: in the DSSYK-dominated chaotic phase the Lanczos coefficients grow linearly with the Krylov level n , and Krylov operator complexity, as well as operator size, exhibits exponential growth in time, whereas in the commuting, quasi-integrable phase the Lanczos coefficients grow only as \sqrt{n} and both Krylov complexity and operator size grow quadratically with time. The change in the Lanczos coefficients and that in Krylov complexity (which follows from the Lanczos coefficients) are the result of interpolating between the quasi-integrable and the chaotic phases by varying the parameter κ in (1.1). Across the first-order transition line determined by the free energy, however, these diagnostics show a polynomial growth and do not show a sharp change of behaviour. In particular, near the transition the scrambling measures in the quasi-integrable and chaotic phases display nearly identical growth in time from the point of view of scrambling as measured by OTOCs and Krylov operator complexity.⁷ We can now answer the question posed above: the phase transition identified in [21, 22] does separate a nearly integrable phase from a genuinely chaotic one, in the sense that deep inside each phase the chaos diagnostics show the expected polynomial versus exponential behaviour. Near the transition line the scrambling measures of the two phases exhibit nearly the same growth in time as measured by Krylov complexity and OTOCs. This is a consequence that at the transition point both the quasi-integrable and the chaotic phases contain similar contributions from the integrable and chaotic chord numbers. However, both of these measures display a discontinuity when the parameter κ (1.1) reaches a critical value, where the first-order phase transition occurs, due to the exchange in the dominating saddle point contribution to the partition function. This means that the quasi-integrable and chaotic phases defined by [21] are not properly integrable nor chaotic in the sense of measures of scrambling; in fact in terms of the scrambling probes, they are nearly indistinguishable near the phase transition line.

⁶Krylov operator complexity can be used as a late time diagnostic of quantum chaos [87]; however, we will only probe time scales comparable or below the scrambling time in this system.

⁷There are certain examples in the literature when Krylov operator complexity in quantum mechanical systems is not a reliable measure of chaos [88–90] at early-times, in contrast to other definitions of quantum chaos, e.g. in terms of level spacing statistics. Nevertheless, Krylov operator complexity can still be reliable at sufficiently late-time regimes [87].

Outline In Sec. 2, we provide a brief introduction to the integrable-chaotic chord Hamiltonian model in [21, 22] and investigate the growth of chord numbers across the integrable-chaotic transition. In Sec. 3, we explore the Krylov basis with respect to the infinite-temperature TFD as the reference state. In Sec. 4, we derive two-point correlation functions and the corresponding Krylov operator complexity for chaotic operators. In Sec. 5, we analyze the operator size growth for the same type of operators at finite temperature. In Sec. 6, we conclude summarizing and interpreting the results; besides mentioning some directions for future research.

We also provide additional details in App. A to complement the background material in Sec. 2; App. B and App. C technical details regarding the Krylov basis in Sec. 3.2.

2 The integrable-chaotic model and its phase transition

In Sec. 2.1, we review the BBJM⁸ model and its chord Hilbert space. In Sec. 2.2, we review its effective action and phase transition in the classical limit. In Sec. 2.3, we present new results regarding the evolution of the chord numbers.

2.1 The BBJM model and its chord Hilbert space

The construction of the chord Hilbert space of the integrable-chaotic chord Hamiltonian (1.1) follows in a similar way to [27], which is reviewed in App. A.4. Let us briefly describe the DSSYK model in some detail. The SYK model is a strongly interacting system of N Majorana fermions ψ_i obeying $\{\psi_i, \psi_j\} = 2\delta_{ij}$ in $(0+1)$ -dimensions with all to all p body interactions (see [3, 85, 86, 91–96] among many others)

$$H_{\text{SYK}}^{(p)} = i^{p/2} \sum_I J_I \Psi_I, \quad (2.1)$$

where I is a collective index indicating $1 \leq i_1 \leq i_2 \leq \dots \leq i_p \leq N$, and we represent $\Psi_I := \psi_{i_1} \dots \psi_{i_p}$; $J_I := J_{i_1, \dots, i_p}$ are random coupling constants which obey the following Gaussian distribution

$$\langle (J_{i_1 \dots i_p}) \rangle = 0, \quad \langle (J_{i_1 \dots i_p})^2 \rangle = N \mathcal{J}^2 \left(2p^2 \binom{N}{p} \right)^{-1}, \quad (2.2)$$

where \mathcal{J} is a constant independent of N and p . The double scaling refers to

$$N, p \rightarrow \infty, \quad \lambda \equiv \frac{2p^2}{N} \text{ fixed.} \quad (2.3)$$

Using the double scaling limit, it can be shown that the ensemble-averaged expectation values of powers of Hamiltonian (2.1) are exactly reproduced by constructing an auxiliary Hilbert space $\mathcal{H} = \text{span}\{|n\rangle\}$, where $|n\rangle$ represent chord-number states (see [22] for a review), and the Hamiltonian acting on \mathcal{H} is denoted \hat{H}_1 .

⁸Additional supplementary material regarding Krylov complexity for states and operators, OTOCs, and about ensemble-averaged doubled-scaled models can be found in App. A.

The commuting SYK model was first proposed in [41], and double-scaled versions of this model have been studied in [21, 22, 24]. A recent extension with multiple commuting DSSYK models, which collectively can describe a chaotic model, was developed in [25].

Meanwhile, the integrable part of (1.1) is constructed by combining N Majorana fermions into Cartan generators of $\text{SO}(N)$, namely the fermion bilinears $iQ_k = \psi_{2k-1}\psi_{2k}$, leading to [21, 22]

$$H_{\text{integrable}}^{(p/2)} = i^{p/2} \sum_{i_1, \dots, i_{p/2}} B_{i_1, \dots, i_{p/2}} Q_{i_1} \dots Q_{i_{p/2}}, \quad (2.4)$$

where we choose a Gaussian distribution of the kind

$$\langle B_{i_1, \dots, i_{p/2}} \rangle = 0, \quad \langle (B_{i_1, \dots, i_{p/2}})^2 \rangle = \mathcal{J}^2 \binom{N/2}{p/2}, \quad (2.5)$$

where we have chosen the overall normalization to involve the same \mathcal{J} parameter as the in the DSSYK for convenience.

We will consider the double scaled limit as in the previous section. The respective auxiliary system spanned by orthonormal chord number states $\{|z\rangle\}$, and the doubled-scaled Hamiltonian is denoted \hat{H}_2 in the auxiliary Hilbert space.

Let the penalty factors between different chord intersections be denoted as follows:

$$H_{\text{SYK}} \cap H_{\text{SYK}} : q_{nn}, \quad H_{\text{SYK}} \cap H_{\text{integrable}} : q_{nz}, \quad H_{\text{integrable}} \cap H_{\text{integrable}} : q_{zz}. \quad (2.6a)$$

The moments of the ensemble averaged Hamiltonian (1.1) can be expressed in terms of chord diagrams as

$$\langle 0 | \hat{H}^k | 0 \rangle = \sum_{\text{chord diagrams}} \nu^n \kappa^z q_{nn}^{\#(H_{\text{SYK}} \cap H_{\text{SYK}})} q_{nz}^{\#(H_{\text{SYK}} \cap H_{\text{integrable}})} q_{zz}^{\#(H_{\text{integrable}} \cap H_{\text{integrable}})}, \quad (2.7)$$

where $k = n + z$; $|0\rangle$ is the zero-chord state, $q_{ij} = e^{-\lambda_{ij}}$ are the intersection weights (here $i, j = \{n, z\}$) are associated with \hat{H}_1 and \hat{H}_2 ; and $\#$ denotes number of intersections. In particular, the *integrable-chaotic* case we have that $q_{nn} = q_{nz} = q$, $q_{zz} = 1$ [21].

The chord diagrams can be used to define an auxiliary Hilbert space for the BBJM model [21, 22] with k chords

$$\mathcal{H}_k = \text{span} \left\{ |n, z; \vec{r}\rangle, \text{ s.t. } \vec{r} = \{0, 1\}, \sum_{i=1}^{k=n+z} r_i = n \right\}, \quad (2.8)$$

with $\dim(\mathcal{H}_k) = 2^k$, and we normalize the corresponding inner-like product [21]

$$\langle\langle n, z; \vec{r} | n', z'; \vec{r}' \rangle\rangle = \delta_{nn'} \delta_{zz'} \delta_{\vec{r}\vec{r}'}. \quad (2.9)$$

In the integrable-chaotic case, the transfer matrix of the ensemble-averaged theory, which plays the role of an effective Hamiltonian, can be written in terms of a q -deformed and a standard harmonic-oscillator algebra acting on the auxiliary Hilbert space of the full system,

$$\hat{H} = \nu(\hat{a}_n + \hat{a}_n^\dagger) + \kappa(\hat{a}_z + \hat{a}_z^\dagger), \quad (2.10)$$

where $\hat{a}_{n/z}^\dagger$ and $\hat{a}_{n/z}$ are the creation and annihilation operators acting on (2.8) as

$$\hat{a}_n |n, z, \vec{r}\rangle = \sqrt{[n]_q} |n-1, z, \vec{r}_1\rangle, \quad \hat{a}_n^\dagger |n, z, \vec{r}\rangle = \sqrt{[n+1]_q} |n+1, z, \vec{r}_2\rangle, \quad (2.11)$$

$$\hat{a}_z |n, z, \vec{r}\rangle = \sqrt{z} |n, z-1, \vec{r}_3\rangle, \quad \hat{a}_z^\dagger |n, z, \vec{r}\rangle = \sqrt{z+1} |n, z+1, \vec{r}_4\rangle, \quad (2.12)$$

where $[n]_q := \frac{1-q^n}{1-q}$, and $\vec{r}_{1 \leq i \leq 4}$ represent different vectors determining the state (2.8). The total chord number operator is defined [21]

$$\frac{1}{\lambda} \hat{l} |n, z, \vec{r}\rangle = (n+z) |n, z, \vec{r}\rangle. \quad (2.13)$$

The two-point function of a normalized chaotic matter operators O (defined in (A.29)) with penalty factor $e^{-\bar{\lambda}}$ with the chaotic chords and integral chords could be computed by chord diagram with,⁹

$$\begin{aligned} G_\Delta(\tau_1, \tau_2) &\equiv \left\langle \text{Tr}[e^{-(\beta+\tau_1)\hat{H}} O e^{-(\tau_1-\tau_2)\hat{H}} O e^{-\tau_2\hat{H}}] / \text{Tr}[1] \right\rangle \\ &= \langle 0 | e^{-(\beta-\tau_2+\tau_1)\hat{H}} e^{-\Delta\hat{l}} e^{-(\tau_2-\tau_1)\hat{H}} | 0 \rangle, \end{aligned} \quad (2.14)$$

where $\Delta = \bar{\lambda}/\lambda$. Due to the time-translational invariance, we have $G_\Delta(\tau_1, \tau_2) = G_\Delta(\tau_{12})$ with $\tau_{12} \equiv \tau_1 - \tau_2$.

2.2 Effective action and phase transition

We will first review the path integral for the variables n and z

$$\langle 0 | e^{-\beta\hat{H}} | 0 \rangle \propto Z_\beta = \int Dn Dz e^{-\frac{1}{\lambda} S}, \quad (2.15)$$

where $n(\tau_1, \tau_2)/\lambda$ and $z(\tau_1, \tau_2)/\lambda$ represent the densities of chaotic and integrable chords connecting points τ_1 and τ_2 in the thermal circle and the effective action is

$$\begin{aligned} S &= \frac{1}{4} \int_0^\beta d\tau_1 \int_0^\beta d\tau_2 \int_{\tau_1}^{\tau_2} d\tau_3 \int_{\tau_2}^{\tau_1} d\tau_4 [n(\tau_1, \tau_2)n(\tau_3, \tau_4) + 2n(\tau_1, \tau_2)z(\tau_3, \tau_4)] \\ &\quad + \frac{1}{2} \int_0^\beta d\tau_1 \int_0^\beta d\tau_2 \left[n(\tau_1, \tau_2) \left(\log \frac{n(\tau_1, \tau_2)}{\nu^2 \mathcal{J}^2} - 1 \right) + z(\tau_1, \tau_2) \left(\log \frac{z(\tau_1, \tau_2)}{\kappa^2 \mathcal{J}^2} - 1 \right) \right], \end{aligned} \quad (2.16)$$

where, in the coarse graining scheme for chords, the steps including (a) Generate, (b) Split, and (c) Reorder, contribute to the second line and the step (d) Cross, contributes to the first line, where we use the terminology in [22].

We consider the classical limit $\lambda \rightarrow 0$ and derive the Liouville equation from the variation principle

$$\begin{aligned} \partial_1 \partial_2 g_n(\tau_1, \tau_2) + 2\nu^2 \mathcal{J}^2 e^{g_n(\tau_1, \tau_2) + g_z(\tau_1, \tau_2)} &= 0, \\ \partial_1 \partial_2 g_z(\tau_1, \tau_2) + 2\kappa^2 \mathcal{J}^2 e^{g_n(\tau_1, \tau_2)} &= 0 \end{aligned} \quad (2.17)$$

⁹This follows similarly to (B.30) in [21] using the corresponding intersection factors between chaotic and integrable chords.

where we introduced the new variables

$$g_n(\tau_1, \tau_2) = - \int_{\tau_1}^{\tau_2} d\tau_3 \int_{\tau_2}^{\tau_1} d\tau_4 n(\tau_3, \tau_4), \quad g_z(\tau_1, \tau_2) = - \int_{\tau_1}^{\tau_2} d\tau_3 \int_{\tau_2}^{\tau_1} d\tau_4 z(\tau_3, \tau_4), \quad (2.18)$$

where $g_n(\tau_1, \tau_2)/\lambda$ and $g_z(\tau_1, \tau_2)/\lambda$ respectively describe the numbers of chaotic and integrable chords going through a line connecting τ_1 and τ_2 . It is convenient to define their sum

$$l(\tau_1, \tau_2) = -(g_n(\tau_1, \tau_2) + g_z(\tau_1, \tau_2)), \quad (2.19)$$

which is the value of chords number operator \hat{l} sandwiched by two states, namely

$$l(\tau_1, \tau_2) = \frac{\langle 0 | e^{-(\tau_2-\tau_1)\hat{H}} \hat{l} e^{-(\tau_1-\tau_2+\beta)\hat{H}} | 0 \rangle}{\langle 0 | e^{-\beta\hat{H}} | 0 \rangle}. \quad (2.20)$$

In the classical limit $\lambda \rightarrow 0$, the two-point function G_Δ of chaotic matter operators O (A.29) are related to the number of chords of both types that cross the chaotic matter chord [21]

$$\lim_{\lambda \rightarrow 0} G_\Delta(\tau_1, \tau_2) = e^{-\Delta l(\tau_1, \tau_2)} = e^{\Delta(g_n(\tau_1, \tau_2) + g_z(\tau_1, \tau_2))}, \quad (2.21)$$

where $g_{n/z}$ and l are defined in (2.18)(2.19) and could be computed by solving (2.17).

Due to time-translational invariance, we have $l(\tau_1, \tau_2) = l(\tau)$ and $g_{n/z}(\tau_1, \tau_2) = g_{n/z}(\tau)$, where $\tau \equiv \tau_1 - \tau_2$. The double-time Liouville equations (2.17) reduce to the equations in terms of τ ,

$$\partial_\tau^2 g_n(\tau) = 2\mathcal{J}^2 \nu^2 e^{g_n(\tau) + g_z(\tau)}, \quad \partial_\tau^2 g_z(\tau) = 2\mathcal{J}^2 \kappa^2 e^{g_n(\tau)}. \quad (2.22)$$

Since no chord going through the connection line when $\tau_1 \rightarrow \tau_2$, the imaginary-time boundary conditions are [21]

$$g_{n/z}(0) = g_{n/z}(\beta) = 0, \quad (2.23)$$

in agreement with the condition of the Euclidean two-point functions $G_\Delta(0) = G_\Delta(\beta) = 1$ via (2.21).

Plugging back the solutions $g_{n/z}$ in the action (2.16) gives the on-shell action

$$S_{\text{on-shell}} = -\frac{1}{4} \int d\tau_1 d\tau_2 \left(\frac{1}{2} g_n \partial_1 \partial_2 g_n + g_n \partial_z \partial_2 g_z + 2(\nu \mathcal{J})^2 e^{g_n + g_z} + (\kappa \mathcal{J})^2 e^{g_n} \right). \quad (2.24)$$

There are three different saddle point solutions to the equations of motion (2.17) depending on κ , corresponding to the quasi-integrable, chaotic and a subleading saddle point. These three solutions lead to a thermodynamic phase transition in terms of the free-energy in the saddle point approximation [21].

We can numerically solve the equation, obtain the solution, and evaluate the on-shell action for various parameters β and κ . We represent the phase transition in Fig. 1.

Next, we consider perturbative solutions about these saddle point solutions, which were previously found in [21].

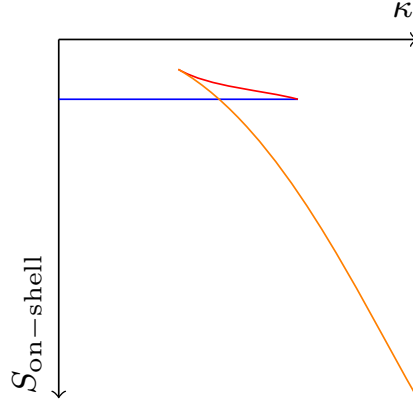


Figure 1. Schematic representation of the phase transition found in [21] (Fig. 11 b) in the on-shell action (2.24) at finite temperature. The blue, red and orange solid lines correspond to the chaotic, a subdominant, and quasi-integrable saddle respectively.

Chaotic saddle For $\kappa \ll 1$, we have as the leading order in κ solution to (2.17) and (2.23):

$$l(\tau) = -2 \log \left[\frac{\cos\left(\frac{\pi\nu}{2}\right)}{\cos\left[\pi\nu\left(\frac{1}{2} - \frac{\tau}{\beta}\right)\right]} \right] + \mathcal{O}(\kappa^4), \quad g_z(\tau) = 2\kappa^2 \log \left[\frac{\cos\left(\frac{\pi\nu}{2}\right)}{\cos\left[\pi\nu\left(\frac{1}{2} - \frac{\tau}{\beta}\right)\right]} \right] + \mathcal{O}(\kappa^4), \quad (2.25)$$

where we have defined

$$\beta\mathcal{J} \equiv \frac{\pi\nu}{\cos\left(\frac{\pi\nu}{2}\right)}. \quad (2.26)$$

Thus, at the leading order, we have $g_z = 0$, and l is simply the single chord solution with (dimensionless) temperature $\beta\mathcal{J}$.

Integrable saddle Similarly, considering $\nu \ll 1$ and low temperatures, $\beta\mathcal{J} \gg 1$, we have as the leading order solutions of (2.17) and (2.23)

$$l(\tau) = -(\mathcal{J}\kappa)^2 \tau (\tau - \beta) + \mathcal{O}\left(\frac{(\beta\mathcal{J})^0}{\kappa^2}\right), \quad g_n(\tau) = \mathcal{O}\left(\frac{\nu^2}{\kappa^4(\beta\mathcal{J})^2}\right). \quad (2.27)$$

So at low temperatures, it is consistent to consider only $l(\tau)$ in (2.25) (2.27) to evaluate the autocorrelation function which will be defined in Sec. 4. We use these saddle point solutions to evaluate the Krylov operator complexity in the next section.

2.3 Evolution of chord numbers

We now evaluate the chord number in (2.19) in Lorentzian signature by implementing a (Hartle-Hawking [97]) analytic continuation at finite temperature: $\tau \rightarrow \beta/2 + it$ in the differential equations (2.17),

$$\partial_t^2 \tilde{g}_n(t) = -2\mathcal{J}^2 \nu^2 e^{\tilde{g}_n(t) + \tilde{g}_z(t)}, \quad (2.28a)$$

$$\partial_t^2 \tilde{g}_z(t) = -2\mathcal{J}^2 \kappa^2 e^{\tilde{g}_n(t)}, \quad (2.28b)$$

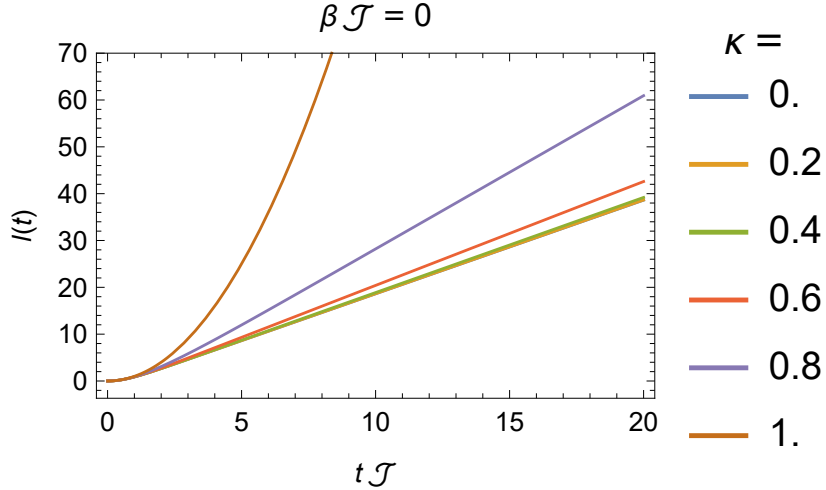


Figure 2. Evolution of $l(t)$ (2.31) along real time, at $\beta\mathcal{J} = 0$ and $\kappa = 0, 0.2, 0.4, 0.6, 0.8, 1.0$. The integrable system limit ($\kappa = 0$) displays the expected parabolic growth; while the chaotic one ($\kappa = 1$) displays late time linear growth, as seen in (2.27) and (2.25) with $\tau = it$ ($\beta = 0$) respectively. Note that the blue, amber and green lines nearly overlap with each other.

where we denote

$$\tilde{g}_{n/z}(t) \equiv g_{n/z}(\tau = \beta/2 + it), \quad (2.29)$$

while the boundary conditions (2.23) are inherently Euclidean. The initial conditions for real time evolution is given by the solution from imaginary time and the time-reversal symmetry

$$\tilde{g}_{n/z}(0) = g_{n/z}(\beta/2), \quad \tilde{g}'_{n/z}(0) = 0. \quad (2.30)$$

where the time-reversal symmetry imply that $\tilde{g}_{n/z}(t) = \tilde{g}_{n/z}(-t)$. Similar to (2.19), we define the rescaled total chord number on real time

$$l(t) \equiv -(\tilde{g}_n(t) + \tilde{g}_z(t)). \quad (2.31)$$

We expect that, at fixed $\beta\mathcal{J}$, the growth rate of the total chord number $l(t)$ increases with increasing κ . As a consequence, the growth in the chaotic phase is slower than that in the quasi-integrable phase. This behavior can be understood from the dominant contributions to the chord number. For small κ , $l(t)$ is dominated by $\tilde{g}_n(t)$, whose evolution is governed by (2.28a). Its growth is strongly constrained by the $e^{\tilde{g}_n(t)}$ damping and therefore remains limited. In contrast, for large κ , $l(t)$ is dominated by $\tilde{g}_z(t)$, whose dynamics is governed by (2.28b). In this regime, the $e^{\tilde{g}_n(t)}$ damping becomes negligible, allowing the chord number to grow more rapidly. This contrast is particularly pronounced at large $\beta\mathcal{J}$, where a strong hierarchy develops between $\tilde{g}_n(t)$ and $\tilde{g}_z(t)$. Consequently, at large $\beta\mathcal{J}$, the chord number grows much faster in the quasi-integrable phase than in the chaotic phase.

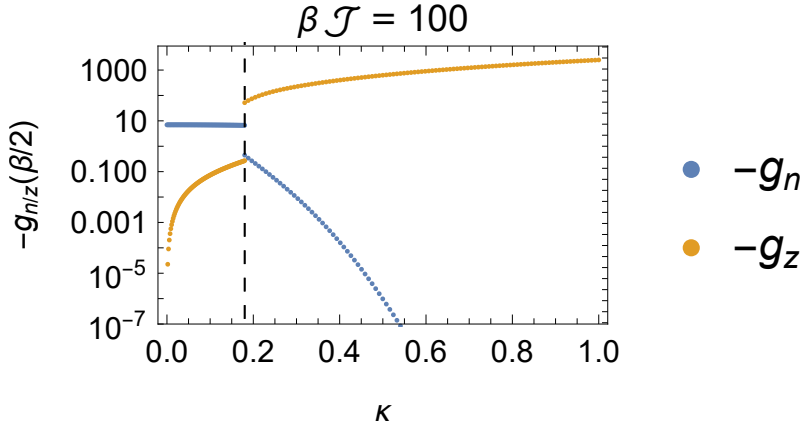


Figure 3. $-g_n(\beta/2)$ and $-g_z(\beta/2)$ (2.18) in the dominating saddle as functions of κ at $\beta\mathcal{J} = 100$. The dashed curve denotes the critical value $\kappa_c = 0.18$. The crossing of $-g_n(\beta/2)$ and $-g_z(\beta/2)$ at κ_c is a consequence of the first-order transition, which shows where the dominant saddle jumps from the chaotic to the quasi-integrable solution.

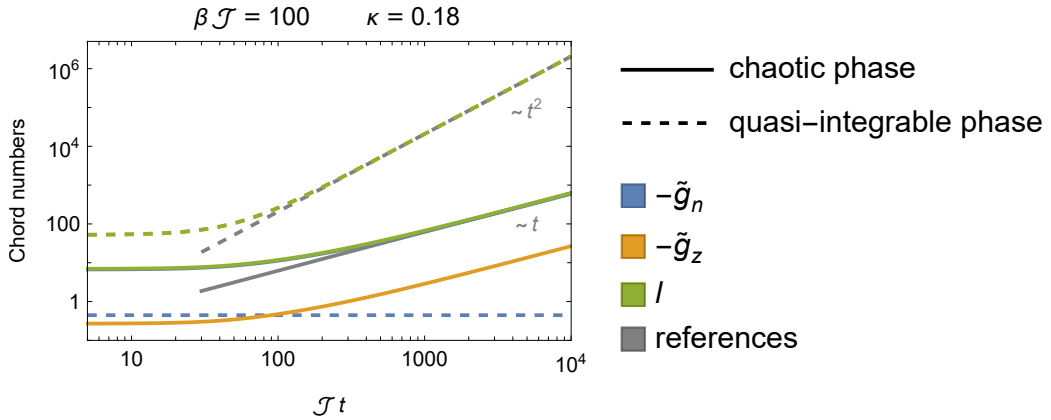


Figure 4. Real time evolution of $l(t) = -\tilde{g}_n(t) - \tilde{g}_z(t)$ in different phases near the phase transition line at $\beta\mathcal{J} = 100$ and $\kappa = 0.18$. The solid blue curve is covered by the green curve and the orange dashed curve is covered by the green dashed curve.

To investigate the growth of the chord number for general $\beta\mathcal{J}$, we first numerically solve the imaginary-time Liouville equation (2.22) with the boundary condition (2.23), and then numerically solve the real-time Liouvillian equation (2.28) with the initial conditions (2.30).

At $\beta\mathcal{J} = 0$, the system undergoes a crossover from the chaotic phase to the quasi-integrable phase as κ increases. Correspondingly, the growth rate of $l(t)$ increases smoothly, and the growth behavior crosses over from linear to quadratic, as shown in Fig. 2.

At $\beta\mathcal{J} = 100$, the imaginary-time solution exhibits a discontinuous jump at the first-order transition point $\kappa_c = 0.18$, as shown in Fig. 3. We then take the solutions on the two sides of the transition as initial conditions and compute their real-time evolutions, respectively. The

results are shown in Fig. 4. In addition to the difference in the magnitude of the chord number, we observe that the chord number grows linearly in the chaotic phase and quadratically in the quasi-integrable phase, indicating a discontinuous change in the growth behavior.

The crossover and the jump in the chord number and its growth behavior are consequences of the thermodynamic crossover and phase transition, respectively. However, the chord number itself does not directly characterize chaos or scrambling. To analyze these properties, one must instead investigate measures of scrambling, such as the Krylov operator complexity and the operator size, across the phase diagram, particularly in the vicinity of the transition line.

3 Discussion on the Krylov basis

We now discuss the Krylov basis of the Krylov state complexity with respect to the infinite-temperature TFD state and show there is a non-trivial limit in which we may identify the total chord number involving integrable and chaotic chords with the Krylov number operator. In Sec. 3.1 we derive the first few Krylov basis in the Lanczos algorithm for general intersection parameter q_{nn} , q_{nz} and q_{zz} . In Sec. 3.2 we specialize in the case $q_{nn} = q_{nz} = q_{zz}$ where we recover a closed form expression for the Krylov basis, Lanczos coefficients, and spread complexity.¹⁰

3.1 General Krylov basis

We consider the monic version of Lanczos algorithm [98] in which the diagonal coefficients a_n do not appear, as the density of states in the partition function are energy eigenvalue-symmetric,

$$|P_{n+1}\rangle = b_{n+1}^{-1}(\hat{H}|P_n\rangle - b_n^2|P_{n-1}\rangle), \quad b_n^2 = \frac{\langle P_n|P_n\rangle}{\langle P_{n-1}|P_{n-1}\rangle} = \langle\langle P_{n-1}|\hat{H}|P_n\rangle\langle P_n|P_{n-1}\rangle. \quad (3.1)$$

Based on this Krylov basis, the Krylov complexity operator is defined by

$$\frac{\hat{l}}{\lambda} = \sum_{k=0}^{\infty} k \frac{|P_k\rangle\langle P_k|}{\langle P_k|P_k\rangle}. \quad (3.2)$$

In the following, we show that when all the Hamiltonian intersections are equal to each other, the Krylov basis $|P_k\rangle$ for the BBJM model can be expanded by the chords states $|n, z, \vec{r}\rangle$ in (2.8) with $k = n + z$ as the total chord number. Starting from

$$|P_0\rangle = |0, 0, \vec{0}\rangle, \quad b_0^2 = 0, \quad (3.3)$$

the Lanczos algorithm leads to

$$\begin{aligned} |P_1\rangle &= \nu|1, 0, \vec{r}_1\rangle + \kappa|0, 1, \vec{r}_2\rangle, \quad b_1^2 = \nu^2 + \kappa^2 = 1, \\ |P_2\rangle &= \nu^2|2, 0, \vec{r}_3\rangle + \nu\kappa|1, 1, \vec{r}_4\rangle = (1, 0) + \nu\kappa|1, 1, \vec{r}_5\rangle = (0, 1) + \kappa^2|0, 2, \vec{r}_6\rangle, \\ b_2^2 &= \nu^4(1 + q_{nn}) + 2\nu^2\kappa^2(1 + q_{nz}) + \kappa^4(1 + q_{zz}) \end{aligned}$$

¹⁰However, given that this case does not describe the integrable-chaotic transition, we will not discuss this part after this section.

where the notation $(0,1,\dots)$ indicates how to build the corresponding \vec{r}_i above. Similar expressions follow for $|P_3\rangle$; however, by computing the overlap between the previous states we obtain

$$\langle\langle 1,0,\vec{r}_1|\hat{H}|P_2\rangle\rangle = \nu [\nu^2(1+q_{nn}) + \kappa^2(1+q_{nz})], \quad (3.4)$$

$$\langle\langle 0,1,\vec{r}_2|\hat{H}|P_2\rangle\rangle = \kappa [\nu^2(1+q_{nz}) + \kappa^2(1+q_{zz})], \quad (3.5)$$

$$\langle\langle 1,0,\vec{r}_1|P_3\rangle\rangle = \nu [\nu^2(1+q_{nn}) + \kappa^2(1+q_{nz}) - b_2^2] \quad (3.6)$$

$$= \nu\kappa^2 [\nu^2(q_{nn} - q_{nz}) + \kappa^2(q_{nz} - q_{zz})],$$

$$\langle\langle 0,1|P_3\rangle\rangle = \kappa [\nu^2(1+q_{nz}) + \kappa^2(1+q_{zz}) - b_2^2] \quad (3.7)$$

$$= \kappa\nu^2 [\nu^2(q_{nz} - q_{nn}) + \kappa^2(q_{zz} - q_{nz})].$$

This implies that we can express

$$|P_3\rangle = \sum_{n+z=3,\vec{r}} \nu^n \kappa^z |n,z,\vec{r}\rangle + |1\text{-chord}\rangle. \quad (3.8)$$

where $|1\text{-chord}\rangle$ denotes a linear combination of $|1,0,\vec{r}_1\rangle$ and $|0,1,\vec{r}_2\rangle$. Note, (3.8) implies that the third element in the Krylov basis corresponds to a one-chord state with and a state with fixed total chaotic and integrable chord number equal to the “position” in the Krylov chain. Iterating the above result for the other elements in the Krylov basis, we expect that $\langle\langle n,z,\vec{r}|P_k\rangle\rangle$ for $n+z \neq k$ is linear in $q_{nn} - q_{nz}$ and $q_{zz} - q_{nz}$. We stress that one can carry out the algorithm above to build the Krylov basis at arbitrary order $|P_n\rangle \forall \kappa \in [0,1]$, but it is technically intricate due to the evaluations involved. However, we expect that the algorithm to higher order will generically lead to an expression where $|P_n\rangle$ is manifestly linearly dependent of lower-order chord states (i.e. $|1\text{-chord}\rangle, \dots |(m < n)\text{-chord}\rangle$).

In addition, we show in App. B that $\{|n,z;\vec{r}\rangle\}$ is not generically a Krylov basis. Nevertheless, we find the full Krylov basis in this system for a special case of the Hamiltonian intersections below.

3.2 Special case: $q_{nn} = q_{nz} = q_{zz}$

When $q_{nn} = q_{nz} = q_{zz}$, we can think of the total Hamiltonian H (1.1) as a superposition of νH_1 chord and κH_2 chord with penalty factor $q_{nn} = q_{nz} = q_{zz}$. Then the H -chord state is the Krylov basis for $|P_0\rangle = |0\rangle$

$$|P_k\rangle = \sum_{n+z=k,\vec{r}} \nu^n \kappa^z |n,z,\vec{r}\rangle \quad (q_{nn} = q_{nz} = q_{zz} = q), \quad (3.9)$$

which means that

$$b_n^2 = \frac{1-q^n}{1-q}, \quad \mu_{2n} = \prod_{m=1}^n b_m^2 = \frac{(q;q)_n}{(1-q)^n}, \quad n \geq 1. \quad (3.10)$$

Therefore, in this regime, the state Krylov complexity is the expectation value of the total chord number operator (3.2). Given that the total chord number corresponds to the position

operator in the Krylov chain, the corresponding Krylov complexity when $q_{nz} = q_{zz} = q_{nn} = q$ is the same as for the DSSYK model, namely (A.30).

Note that by the choice $q_{nz} = q_{zz} = q_{nn} = q$ the configuration essentially corresponds to a system of two decoupled DSSYK models of different colors.¹¹ However, this system does not describe the BBJM model. Instead, the spread complexity follows just as in the DSSYK model. For completeness, we analyze deviations from the Krylov basis with $q_{nz} = q_{zz} = q_{nn}$ in App. C.

4 Krylov operator complexity across the phase transition

We now derive the Krylov operator complexity to diagnose the scrambling. In Sec. 4.1 we apply our results to compute Krylov operator complexity based on the moment method, where the normalized autocorrelation functions determine Krylov complexity. In Sec. 4.2 we evaluate Krylov operator complexity perturbatively based on the corresponding two-point functions.

4.1 Krylov operator complexity

As the initial operator in the Krylov approach, we consider a light operator O with $\Delta \rightarrow 0$ in the center of a half thermal circle, namely $O_\beta = e^{-\beta \hat{H}/4} O e^{-\beta \hat{H}/4}$. In the Liouville operator Hilbert space, we denote by $|O_\beta\rangle$ the state corresponding to the operator O_β , with inner product $\langle A|B\rangle \equiv \text{tr}(A^\dagger B)$, so that $\langle O_\beta|O_\beta\rangle = \text{tr}(O_\beta^\dagger O_\beta)$. Its normalized autocorrelation function is

$$G(t) = \frac{\langle O_\beta|e^{i\hat{L}t}|O_\beta\rangle}{\langle O_\beta|O_\beta\rangle} = 1 + \Delta (l(t) - l(0)) + \dots = e^{\Delta(l(t) - l(0))} + \dots \quad (4.1)$$

where the ellipsis represents higher order terms. We construct the moments as

$$\mu_n = \frac{\langle O_\beta|\hat{L}^n|O_\beta\rangle}{\langle O_\beta|O_\beta\rangle} = (-i)^n G^{(n)}(0) = \begin{cases} 1, & n = 0, \\ (-i)^n \Delta l^{(n)}(t=0), & n \geq 1. \end{cases} \quad (4.2)$$

Based on the Liouville equation in real time (2.28) we now calculate all the derivatives $\tilde{g}_{n/z}^{(n)}(0)$ from the iterative equations at $t = 0$ where the superindex $^{(n)}$ indicates the n -th derivative with respect to t ,

$$\tilde{g}_n^{(n+2)}(0) = -2\mathcal{J}^2 \nu^2 B_n(l^{(1)}(0), l^{(2)}(0), \dots, l^{(n)}(0)) e^{l(0)}, \quad (4.3)$$

$$\tilde{g}_z^{(n+2)}(0) = -2\mathcal{J}^2 \kappa^2 B_n(\tilde{g}_n^{(1)}(0), \tilde{g}_n^{(2)}(0), \dots, \tilde{g}_n^{(n)}(0)) e^{\tilde{g}_n(0)}, \quad (4.4)$$

$$l^{(n)}(0) = -\tilde{g}_n^{(n)}(0) - \tilde{g}_z^{(n)}(0), \quad (4.5)$$

¹¹DSSYK systems with several colors have attracted interest in the literature [23, 25] motivated by experimental progress in quantum teleportation protocols in quantum computing [42].

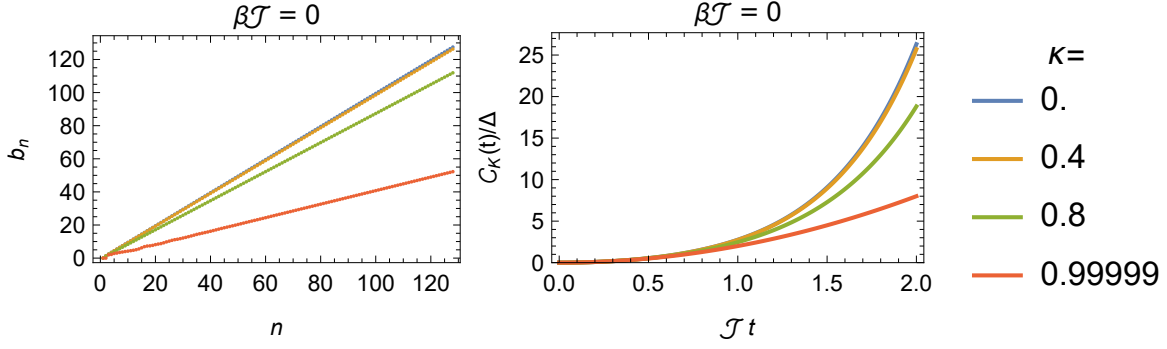


Figure 5. (Left) The Lanczos coefficients b_n at $\beta\mathcal{J} = 0$ for different values of κ in the $\Delta \rightarrow 0$ limit. (Right) Krylov complexity for matter chord operators for different values of κ while keeping $\beta\mathcal{J} = 0$. Note that the complexity of largest value of κ already converges to the result in (4.13). At $\beta\mathcal{J} = 0$, the Lanczos coefficients and Krylov complexity interpolate from chaotic behaviour at small κ to integrable behaviour at large κ . Note there is no phase order transition due to the infinite temperature limit. In the left figure, the blue, amber and green set of dots are nearly coincident, while on the right the blue and brown solid curves are nearly coincident with each other.

starting from the initial condition $\tilde{g}_{n/z}(0) = g_{n/z}(\beta/2)$, $\tilde{g}'_{n/z}(0) = 0$, where $B_n(x_1, x_2, \dots, x_n)$ is the complete Bell polynomial. We carry this out numerically for general ν, κ and β . We find $\tilde{g}_{n/z}^{(n)}(0) = 0$ for odd n , such that $\mu_n = 0$ for odd n . We then calculate the moments μ_{2n} for $n \leq n_c$. In the $\Delta \rightarrow 0$ limit, $\mu_n, \forall n \geq 2$ is linear in Δ . From the truncated moments and their Hankel matrix $H_n = \{\mu_{i+j}\}_{0 \leq i, j < n}$, we calculate the truncated Lanczos coefficients as

$$a_n = 0, \quad b_1^2 = \det H_0, \quad b_n^2 = \frac{\det H_n \det H_{n-2}}{(\det H_{n-1})^2}, \quad n \leq n_c. \quad (4.6)$$

We implement the above algorithm with exact numbers up to $n_c = 60$ or high-precision numbers up to $n_c = 128$. When $\kappa < 1$, except for $b_1 = \sqrt{2\Delta}$, the b_n for $n \geq 2$ are order Δ^0 . When $\beta\mathcal{J} = 0$, the Lanczos coefficients for some κ are shown in the left panel of Fig. 5. The Lanczos coefficients b_n grow linearly for small κ with a slope negatively related to κ . When $\beta\mathcal{J} = 100$, with $\kappa_c \approx 0.18$, the Lanczos coefficients in each phase are shown in the left panel of Fig. 6. The results displays the expected interpolation between the $\propto n$ growth for a chaotic and $\propto \sqrt{n}$ growth for an integrable system.

Then we can construct the tridiagonal form of the Liouvillian $\hat{\mathcal{L}}$, which is a $(n_c+1) \times (n_c+1)$ matrix. Starting from the initial state $\varphi_n(0) = \delta_{n0}$, the Krylov wave function is

$$\varphi_m(t) = \sum_{n=0}^{n_c} \left(e^{i\hat{\mathcal{L}}t} \right)_{mn} \varphi_n(0). \quad (4.7)$$

This truncation is valid in a finite period, when $n_c |\varphi_{n_c}(t)|^2$ is still negligible. Finally, we can

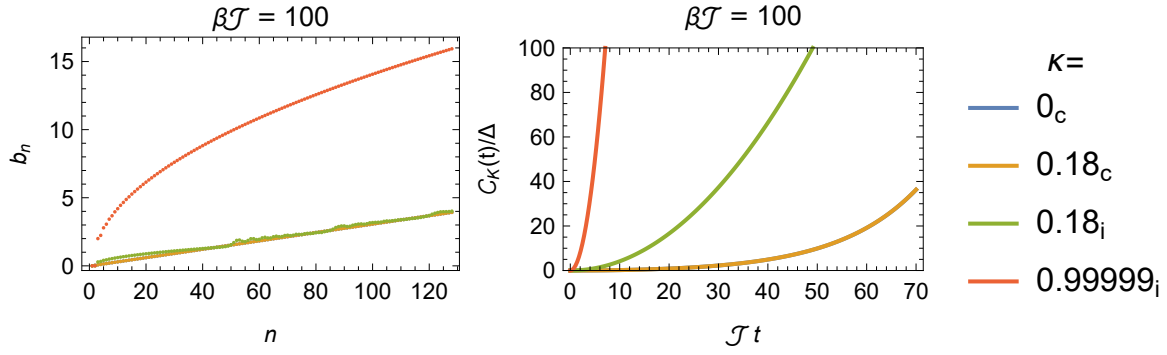


Figure 6. (Left) The Lanczos coefficients b_n at $\beta\mathcal{J} = 100$ for different value of κ in the $\Delta \rightarrow 0$ limit. The subscripts in the values of κ labels the corresponding phases, where c refers to chaotic phase and i refers to quasi-integrable phase. Blue, amber and green dots are nearly coincident with each other. (Right) Krylov complexity for matter chord operators for different values of κ while keeping $\beta\mathcal{J} = 100$. In both of panels, the blue dots (left) and curves (right) are covered by the amber ones curves. The results confirm there is a jump in Krylov operator complexity at the chaotic to integrable phase transition.

calculate the Krylov complexity from

$$\mathcal{C}_K(t) = \sum_{n=0}^{n_c} n |\varphi_n(t)|^2. \quad (4.8)$$

We find that $\mathcal{C}_K(t)/\Delta$ converges to finite values when $\Delta \rightarrow 0$. When $\beta\mathcal{J} = 0$, the Krylov complexity in the valid period are shown in the right panel of Fig. 5. The Krylov complexity exhibits the crossover from exponential growth to quadratic growth with a *decreasing* growth rate as κ increases, namely, the system goes from chaotic region to integrable region. When $\beta\mathcal{J} = 100$, the Krylov complexity in the valid period are shown in the right panel of Fig. 6. The Krylov complexity exhibits a crossover from exponential growth to quadratic growth with an increasing growth rate as κ increases.

4.2 Perturbative approach to Krylov operator complexity

In this section, we investigate the limiting behavior of Krylov operator complexity when the system is very far from the phase transition line, corresponding to $\kappa \ll 1$ for the chaotic and $\nu \ll 1$ the quasi-integrable phases, as seen below. The analytical expressions of the complexity presented here support our numerical complexity dynamics far from the transition point as shown in Fig. 6.

Chaotic saddle To compute the Krylov complexity, we apply Euclidean continuation in (2.25) by $\tau \rightarrow it + \frac{\beta}{2}$ [43], which then gives:

$$l = -2 \log \left[\frac{\cos\left(\frac{\pi v}{2}\right)}{\cosh\left[\frac{\pi v t}{\beta}\right]} \right] + \mathcal{O}(\kappa^4), \quad \tilde{g}_z = 2\kappa^2 \log \left[\frac{\cos\left(\frac{\pi v}{2}\right)}{\cosh\left[\frac{\pi v t}{\beta}\right]} \right] + \mathcal{O}(\kappa^4), \quad (4.9)$$

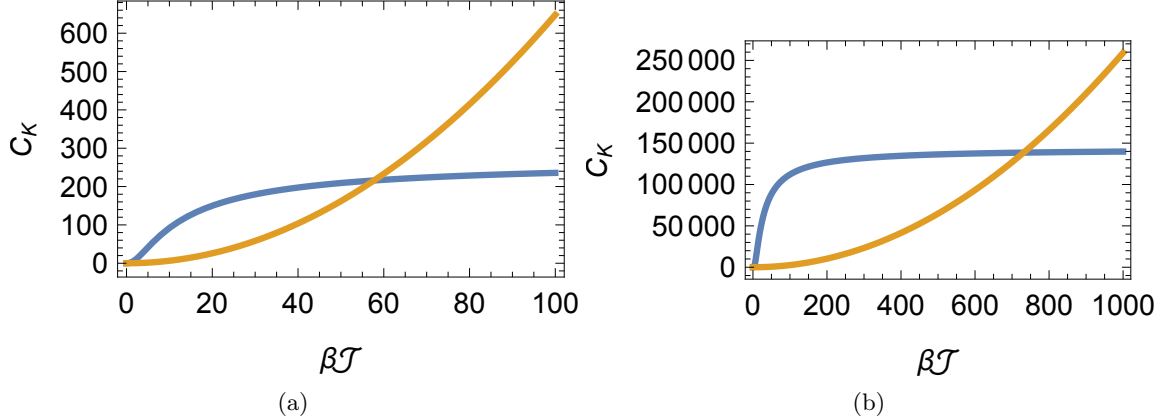


Figure 7. Krylov operator complexity for chaotic operator, $\mathcal{C}_K(t)$, for the approximate chaotic saddle point (4.11) (blue) and quasi-integrable (4.13) (orange) approximate saddle point, as a function of $\beta\mathcal{J}$ with $\kappa = 0.24$ and $t = 1$ (left) or $t = 2$ (right).

where β is defined in (2.26). Next, we evaluate the normalized autocorrelation function (2.21) to $\mathcal{O}(\kappa^2)$:

$$\varphi_0(t) = \frac{G_\Delta(t)}{G_\Delta(0)} = \operatorname{sech}^2 \left[\frac{\pi v t}{\beta} \right] + \mathcal{O}(\kappa^2). \quad (4.10)$$

The Lanczos coefficients b_n and Krylov operator complexity this type of correlator (4.9) can be found in [99]

$$b_n \approx \frac{\pi v}{\beta} \sqrt{n(2\Delta + n - 1)}, \quad \mathcal{C}_K(t) \approx 2\Delta \sinh^2 \left(\frac{\pi v t}{\beta} \right). \quad (4.11)$$

The result is in agreement with the numerical results in Fig. 6, which also displays exponential growth of Krylov operator complexity when $\kappa \ll 1$. This is expected for the operator growth hypothesis [7], since we have a chaotic system with a Lyapunov exponent $\pi v/\beta$ (i.e. it saturates the bound in [100] only when $v = 1$ as defined in (2.26)).¹²

Integrable saddle Implementing the rotation $\tau \rightarrow it + \frac{\beta}{2}$ in (2.27) and evaluating up to order $\mathcal{O}(\frac{\nu^2}{\kappa^4(\beta\mathcal{J})^2})$, we get

$$\varphi_0(t) = \frac{G_\Delta(t)}{G_\Delta(0)} = \exp \left[-\Delta (\mathcal{J}\kappa t)^2 \right]. \quad (4.12)$$

This is essentially the autocorrelation function in a harmonic oscillator, whose Krylov complexity has been studied in [99]

$$b_n = \mathcal{J}\kappa \sqrt{2\Delta n}, \quad \mathcal{C}_K(t) = 2\Delta (\mathcal{J}\kappa t)^2. \quad (4.13)$$

¹²However, given that the DSSYK has a bounded energy spectrum, the late time Krylov complexity should have late time linear growth [101], which can be most straightforwardly shown from the one-particle chord Hilbert space in the pure DSSYK model [38, 40, 102, 103]. It would be interesting to formulate particle Hilbert space in this model, which we leave for future directions.

The result is consistent with Fig. 6 which also shows a parabolic growth when $\nu \ll 1$. The result is due to the fact that the integrable system is essentially a harmonic oscillator.

We illustrate the behavior of Krylov operator complexity for the integrable (4.13) and chaotic (4.11) approximate saddle points, which we illustrate in Fig. 7.

5 Operator size growth across the phase transition

We now test the integrable-chaotic transition through the operator size growth at finite temperature, which is linearly related to an OTOC [104]. This can be computed by solving Liouville equations in the presence of twisted boundary conditions in the classical limit at all temperatures [105, 106] (reviewed in App. A.3). However, due to the interpolating Hamiltonian (1.1), we have to rederive the twisted boundary conditions of the variables g_n and g_z of two kinds of chords from the effective action (2.16).

Based on the double-copy Hilbert space of the N Majorana fermions and the left-and-right copies of operators [107], we introduce the size operator \hat{s} which will be related to the chord number operator (3.2)

$$\hat{s} = \frac{1}{2} \sum_{j=1}^N (1 + i\psi_j^L \psi_j^R). \quad (5.1)$$

We can define the size of an operator O [104] as

$$s[O] \equiv \frac{\langle \text{EPR} | O_L^\dagger \hat{s} O_L | \text{EPR} \rangle}{\langle \text{EPR} | O_L^\dagger O_L | \text{EPR} \rangle} \quad (5.2)$$

where $|\text{EPR}\rangle$ is the maximally entangled state between the double-copy Hilbert space, defined by $(\psi_j^L + i\psi_j^R) |\text{EPR}\rangle = 0$. The expectation value on $|\text{EPR}\rangle$ result in a normalized trace in the single-copy Hilbert space, such as the thermal partition function

$$\langle \text{EPR} | e^{-\beta \hat{H}_{LR}/2} | \text{EPR} \rangle = \text{Tr}[e^{-\beta \hat{H}}]/\text{Tr}[1], \quad (5.3)$$

where $\hat{H}_{LR} = \hat{H}_L + \zeta \hat{H}_R$, $\hat{H}_L |\text{EPR}\rangle = \zeta \hat{H}_R |\text{EPR}\rangle$ and $\zeta = (-1)^{p/2}$.

We will focus on the operators $e^{-\beta \hat{H}/2}$ and $O_\beta(t) = e^{-\beta \hat{H}/4} O(t) e^{-\beta \hat{H}/4}$, where O is a normalized chaotic matter operator (defined in (A.29)) composed of s_O Majorana fermions in each of its terms. Consequently, its operator size [108] satisfies $s[O] = s_O$. We will consider the scaling $s_O \sim 1$ in the classical limit $\lambda \rightarrow 0$ such that its scaling dimension $\Delta = \bar{\lambda}/\lambda = s_O/p \sim 1/p$.

To compute the size of the operator $O_\beta(0)$, we define the size generating function by introducing the twisted operator $e^{-\mu \hat{s}}$ in (5.3), namely

$$\langle \text{EPR} | e^{-\beta \hat{H}_{LR}/4} e^{-\mu \hat{s}} e^{-\beta \hat{H}_{LR}/4} | \text{EPR} \rangle, \quad (5.4)$$

which corresponds to the insertion of an twisted boundary condition in the thermal circle [105]. We insert the Majorana fermions ψ_j^L and ψ_j^R inside \hat{s} at locations $\tau = \frac{3\beta}{4}$ and $\frac{\beta}{4}$ along the thermal circle $[0, \beta)$ respectively.

In the double-scaling limit, the operator size in the disorder average is proportional to the chord number [107], namely,

$$\frac{1}{p} \langle s[O] \rangle_J \xrightarrow[\text{limit}]{\text{double-scaling}} \frac{1}{\lambda} \frac{\langle 0 | \tilde{\mathcal{O}} \hat{l} \tilde{\mathcal{O}} | 0 \rangle}{\langle 0 | \tilde{\mathcal{O}} \tilde{\mathcal{O}} | 0 \rangle}, \quad (5.5)$$

where $\langle \cdot \rangle_J$ trace over the fermions and ensemble averaging over the couplings; the chord number operator \hat{l}/λ in (3.2) defined in the chord space measures the number of chords going through the line connecting the locations $\tau = \frac{\beta}{4}, \frac{3\beta}{4}$ of the two Majorana fermions ψ_j^L, ψ_j^R in the chord diagram. $\tilde{\mathcal{O}}$ is a operator acting on the chord space that corresponds to the operator O in the SYK model.

The insertion in (5.4) results in an additional term in the effective action (2.16)

$$S' = S + \tilde{\mu} l\left(\frac{3\beta}{4}, \frac{\beta}{4}\right), \quad (5.6)$$

where $\tilde{\mu} = \mu p$. So the eigenvalue of \hat{l} is $l\left(\frac{3\beta}{4}, \frac{\beta}{4}\right)$ defined in (2.19). Following the derivation in Sec. 2.2, the additional term leads to the deformed Liouville equation

$$\begin{aligned} \partial_1 \partial_2 g_n(\tau_1, \tau_2) + 2\nu^2 \mathcal{J}^2 e^{g_n(\tau_1, \tau_2) + g_z(\tau_1, \tau_2) - \tilde{\mu} \theta(\tau_1, \tau_2)} &= 0, \\ \partial_1 \partial_2 g_z(\tau_1, \tau_2) + 2\kappa^2 \mathcal{J}^2 e^{g_n(\tau_1, \tau_2) - \tilde{\mu} \theta(\tau_1, \tau_2)} &= 0, \end{aligned} \quad (5.7)$$

where

$$\theta(\tau_1, \tau_2) = \begin{cases} 1, & \left(\tau_1 \in \left(-\frac{\beta}{4}, \frac{\beta}{4}\right) \wedge \tau_2 \in \left(\frac{\beta}{4}, \frac{3\beta}{4}\right)\right) \vee \left(\tau_1 \in \left(\frac{\beta}{4}, \frac{3\beta}{4}\right) \wedge \tau_2 \in \left(-\frac{\beta}{4}, \frac{\beta}{4}\right)\right), \\ 0, & \text{others,} \end{cases} \quad (5.8)$$

up to the periodicity $\tau \sim \tau + \beta$. The boundary conditions, with the corresponding symmetries from (5.6), are

$$g_{n/z}(\tau, \tau) = 0, \quad (5.9a)$$

$$g_{n/z}(\tau_1, \tau_2) = g_{n/z}(\tau_1 + \beta, \tau_2) = g_{n/z}(\tau_1, \tau_2 + \beta), \quad (5.9b)$$

$$g_{n/z}(\tau_1, \tau_2) = g_{n/z}^*(-\tau_2, -\tau_1) = g_{n/z}^*\left(\frac{\beta}{2} - \tau_2, \frac{\beta}{2} - \tau_1\right) = g_{n/z}\left(\tau_2 + \frac{\beta}{2}, \tau_1 + \frac{\beta}{2}\right). \quad (5.9c)$$

The fundamental domain can then be chosen as the diamond

$$(0 < \tau_1 + \tau_2 < \frac{\beta}{2}) \cap (0 < \tau_1 - \tau_2 < \frac{\beta}{2}). \quad (5.10)$$

Once we solve (5.7) with the boundary conditions, we obtain the two-point function of O in the presence of the insertion of $e^{-\mu \hat{s}}$. For example,

$$e^{-\Delta l_\mu(\beta/2, 0) - \mu s_O} = \frac{\langle \text{EPR} | O_L e^{-\beta \hat{H}_{LR}/4} e^{-\mu \hat{s}} e^{-\beta \hat{H}_{LR}/4} O_L | \text{EPR} \rangle}{\langle \text{EPR} | e^{-\beta \hat{H}_{LR}/4} e^{-\mu \hat{s}} e^{-\beta \hat{H}_{LR}/4} | \text{EPR} \rangle}, \quad (5.11)$$

where the subscript “ μ ” denotes the solution of $l(\tau_1, \tau_2)$ (where $-l = g_n + g_z$) in the Liouville equation (5.7) in the presence of insertion $e^{-\mu \hat{s}}$.

To compute the OTOC or operator size along real time, we should further introduce an analytical continuation in the numerator of (5.11)

$$\langle \text{EPR} | e^{-(\beta/4+it)\hat{H}_L - (\beta/4-it)\zeta\hat{H}_R} e^{-\mu\hat{s}} e^{-(\beta/4-it)\hat{H}_L - (\beta/4+it)\zeta\hat{H}_R} | \text{EPR} \rangle, \quad (5.12)$$

which result in a deformation in the time contour

$$(0, \beta) \rightarrow (0, \frac{\beta}{4} + it) \cup (\frac{\beta}{4} + it, \frac{\beta}{2}) \cup (\frac{\beta}{2}, \frac{3\beta}{4} + it) \cup (\frac{3\beta}{4} + it, \beta) \quad (5.13)$$

in the effective action (2.16). Instead of changing the time contour, we simply replace the only dimensionful coupling \mathcal{J}^2 in the original effective action (2.16) and the Liouville equation (5.7) with

$$\mathcal{J}^2 \rightarrow \mathcal{J}^2 f(\tau_1) f(\tau_2), \quad (5.14)$$

where

$$f(\tau) = \begin{cases} 1 - i4t/\beta, & \tau \in (0, \frac{\beta}{4}) \cup (\frac{\beta}{2}, \frac{3\beta}{4}), \\ 1 + i4t/\beta, & \tau \in (\frac{\beta}{4}, \frac{\beta}{2}) \cup (\frac{3\beta}{4}, \beta). \end{cases} \quad (5.15)$$

After we replace the coupling while preserving the time contour, the fundamental domain (5.10), as well as the boundary conditions and symmetries in (5.9), remain unchanged. By solving the Liouville equations (5.7) under the replacement (5.14) with the boundary conditions (5.9), we obtain the real-time two-point function in the presence of insertion. For example,

$$e^{-\Delta l_\mu(\beta/2,0) - \mu s_O} = \frac{\langle \text{EPR} | O_L e^{-(\beta/4+it)\hat{H}_L - (\beta/4-it)\zeta\hat{H}_R} e^{-\mu\hat{s}} e^{-(\beta/4-it)\hat{H}_L - (\beta/4+it)\zeta\hat{H}_R} O_L | \text{EPR} \rangle}{\langle \text{EPR} | e^{-\beta\hat{H}_{LR}/4} e^{-\mu\hat{s}} e^{-\beta\hat{H}_{LR}/4} | \text{EPR} \rangle}. \quad (5.16)$$

Given that the resulting Liouville equations may acquire complex coefficients from (5.15), in general, the solution $l_\mu(\tau_1, \tau_2)$ is complex-valued. The change in operator size is given by

$$\Delta_\beta s(t) := s[O_\beta(t)] - s[e^{-\beta\hat{H}/2}] = s_O(1 + \partial_{\tilde{\mu}} l_\mu(\beta/2, 0)|_{\tilde{\mu}=0}). \quad (5.17)$$

To extract the chaotic characteristic in the operator size, we will be only interested in the relative size growth

$$\delta s(t) := \frac{\Delta_\beta s(t) - \Delta_\beta s(0)}{s_O} = \partial_{\tilde{\mu}} l_\mu(\beta/2, 0)|_{\tilde{\mu}=0}. \quad (5.18)$$

Next, we solve the Liouville equations (5.7) numerically using a finite-difference method. Throughout, we fix $1/(\beta\mathcal{J}) = 0.06$, scan $\kappa \in [0, 1]$, where the phase transition occurs at $\kappa = 0.42$. Due to numerical instability, we are only able to obtain solutions up to $t\mathcal{J} < 10$ in

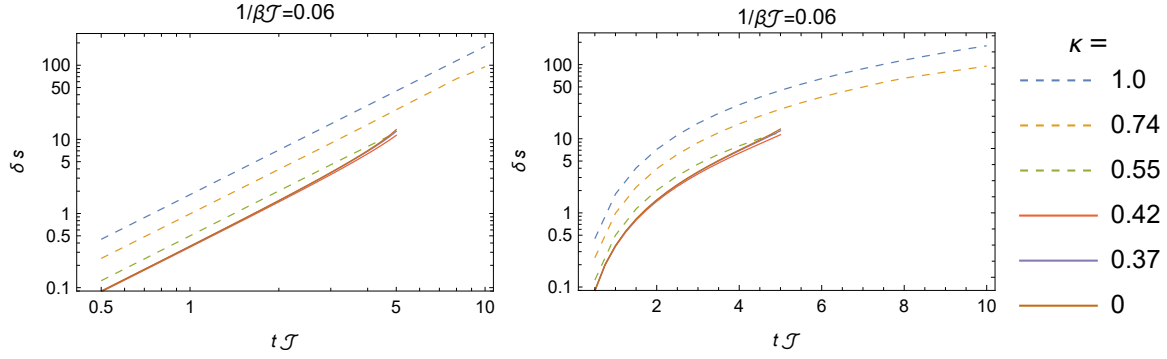


Figure 8. The relative size growth δs as functions of time for $\kappa = 1.0, 0.74, 0.55, 0.42, 0.37, 0$ in the log-log plot and the log plot, where the dashed and solid curves indicate κ in the quasi-integrable and chaotic phases respectively. The relative size growth $\delta s(t)$ is power-law (approximately t^2) deep in the quasi-integrable phase and cosh/exponential-like in the chaotic phase, but the curves become very similar near κ_c , demonstrating that size growth does not show a qualitative change.

the quasi-integrable phase ($0.42 < \kappa \leq 1$) and up to $tJ < 5$ in the chaotic phase ($0 \leq \kappa < 0.42$). From this, we extract the relative size growth $\delta s(t)$ in (5.18) by computing the difference around $\tilde{\mu} \approx 0$. The resulting relative size growth is shown in Fig. 8 within the accessible regions.

Away from the phase transition, we observe power-law growth $\delta s \propto t^\eta$ with $\eta \approx 2.0$ in the quasi-integrable phase, and hyperbolic-cosine growth $\delta s \propto \cosh(\lambda_L t) - 1$ with $\lambda_L \approx 0.5$ in the chaotic phase. However, near the phase transition point, the size growth displays no qualitative change rather than a significant change between power-law and exponential behaviour. These numerical observations for the size growth are consistent with our results on Krylov operator complexity. The characteristic signatures of scrambling appear only deep within the quasi-integrable or chaotic phases, and do not undergo a sharp change at the phase transition point in terms of the difference in operator size (5.18). However, there is still a discontinuity in the OTOC itself since it involves the total chord number (5.16). Thus, both methods suggest the two phases behave in a very similar way near the first-order transition line.

6 Discussion

In this work, we considered the chord Hamiltonian model of [21, 22] and used the Krylov complexity and operator size at finite temperature to probe scrambling properties across the thermodynamic phase transition. This transition is referred to as the integrable-chaotic transition in [21], as it interpolates between a chaotic model and an integrable model.

We find that deep inside the quasi-integrable phase and the chaotic phase, the dominant saddle behaves in a manner naturally described as integrable on one side and chaotic on the other, as reflected in the behavior of the Lanczos coefficients and the growth of operator size. However, upon crossing the first-order transition by varying the parameter κ in the

Hamiltonian (6.1), these chaos diagnostics do not exhibit a sharp transition, in contrast to the discontinuity observed in the dynamics of the chord number, which is controlled by the thermodynamic phase transition.

Our main outcome is that while the model does interpolate between integrable and chaotic behavior, and the Krylov complexity and operator size do capture this change as a thermodynamic transition, the first-order thermodynamic phase transition identified as separating the quasi-integrable and chaotic phases in [21] does not necessarily correspond to a sharp transition between integrability and chaos as diagnosed by scrambling measures.

Meanwhile, regarding spread complexity in this model, we found that there are technical difficulties in deriving the Krylov basis in full generality. The main reason for this difficulty is that the chord basis contains a vector denoted by \vec{r}_i which depends on how many and in what order the integrable and chaotic chord creation operators are introduced to generate the state. This results in a non-trivial construction of the Krylov basis. Nevertheless, we included an algorithm to evaluate the Krylov basis, which can be applied iteratively. We found that the basis can still be solved under specific regimes determined by the Hamiltonian intersection weights, when the expectation value of the total chord number including the integrable and chaotic models reproduces the Krylov state complexity. On the other hand, the evaluation of the Krylov operator complexity and operator size were carried out by solving the Liouvillian equations for the integrable and chaotic chord numbers. Importantly, the chaotic and integrable contributions to the total operator size with general κ display a similar growth as for the purely chaotic ($\kappa = 0$) and integrable ($\kappa = 1$). Thus, both Krylov operator complexity and the finite temperature OTOCs confirm that the classification in integrable and chaotic phases in [21, 22] is valid, even though they display similar behaviour to each other near the transition line.

Below, we comment on future directions.

6.1 Outlook

Towards the bulk dual As emphasized in the introduction, there are significant pieces of evidence that point to sine dilaton gravity being dual to the DSSYK model. It was also realized in [24] that the integrable chord theory can be interpreted as the DSSYK model at high temperatures, and it can be described by sine dilaton gravity in its flat space limit [44] (namely, flat space JT gravity [109, 110]). Based on these relations, a natural expectation for the bulk dual theory of the BBJM model is that it corresponds to

$$I = \nu I_{\text{SD}} + \kappa I_{\text{flat-JT}},$$

$$I_{\text{SD}} = -\frac{1}{16\pi G_N} \left(\int_{\mathcal{M}} d^2x \sqrt{g} (\Phi \mathcal{R} + 2 \sin \Phi) + 2 \int_{\partial\mathcal{M}} dx \sqrt{h} (\Phi_B K - \text{counterterm}) \right), \quad (6.1)$$

$$I_{\text{flat-JT}} = -\frac{1}{16\pi G_N} \left(\int_{\mathcal{M}} d^2x \sqrt{g} \Phi \mathcal{R} + 2 \int_{\partial\mathcal{M}} dx \sqrt{h} (\Phi_B K - \text{counterterm}) \right),$$

where \mathcal{M} is the manifold, G_N Newton's constant, \mathcal{R} the Ricci scalar, K the mean curvature at $\partial\mathcal{M}$, $g_{\mu\nu}$ the metric in \mathcal{M} , h_{mn} the induced metric in $\partial\mathcal{M}$, Φ_B the value of the dilaton at

the boundary.

To be able to interpret our results holographically, we need to evaluate bulk observables, specifically minimal geodesic length connecting the asymptotic boundaries in the corresponding background solutions to the bulk theory (6.1). In sine dilaton gravity, the minimal geodesic length is indeed known to be dual to Krylov operator complexity for the DSSYK model [103], and similarly the chord number in the double-scaled commuting SYK model can be interpreted in terms of a geodesic length between the asymptotic boundaries of the dual geometry [24]. Another relation between Krylov complexity and bulk geometry has been recently put forward in a series of works relating the rate of growth of Krylov complexity with the proper radial momentum of a probe particle [111, 112] (see also [38, 113–116]) and Krylov operator complexity of the DSSYK model with matter chords [116]. It would be interesting to develop the holographic interpretation of the corresponding observables in this work. On the other hand, we also expect that OTOCs in the bulk theory (6.1) with a scalar wordline particle would match our results in Sec. 5. To make progress in this direction, we might apply recent lessons from [49]. The authors find that OTOCs can be computed in sine dilaton gravity by evaluating end-of-the-world branes. It might be possible to implement the gluing and splitting procedure in [49] for the theory (6.1) with matter insertion to investigate the integrable-chaotic transition from the bulk perspective.

Finite N realization In this work, we focused on appropriate measures of chaos for strictly $N \rightarrow \infty$ systems. However, there are several useful measures of chaos for $N \gg 1$ but finite. For instance, the level spacing statistics can be used as a definition integrability, quantum chaos or something in between. The spectral form factor [3] is another measure with great relevance, which could be used to confirm some of the outcomes in this study by discerning between integrable and chaotic behaviour near the phase transition, depending how one approaches it in the phase diagram. Moreover, there are closely connected systems, such as the Rosenzweig-Porter model that also contains a chaotic Hamiltonian, i.e. obeying random matrix statistics, and an integrable Hamiltonian that are decoupled. The connection with the DSSYK model is more explicit when we consider its $q \rightarrow 0$ limit, given that it recover a similar random matrix theory behaviour [28]. To make a meaningful comparison, one might try to pick appropriate large values for N and p in a single realization of the SYK that mimic those of the DSSYK model; and similarly for the Rosenzweig-Porter and BBJM models. Useful numerical results in this direction can be found e.g. [117, 118].¹³ This could allow us to study the chaos-integrability transition with other chaos measures. For instance, there are other important characteristics about the Rosenzweig-Porter model that can be deduced from the inverse participation ratio in Krylov complexity, which measures the degree of localization [20], and (multi)fractality in the system [119]. We are preparing a detailed study about these models to highlight their connection.

¹³We thank Micha Berkooz for useful discussions about this.

Local quenches One might also consider how the two-point functions evaluated in Sec. 4 are modified due to local quenches explicitly altering the Hamiltonian evolution at a given initial time $t = t_0$:

$$|\psi(t)\rangle = \begin{cases} e^{-it\hat{H}}|_{\kappa=\kappa_1} |\psi_0\rangle, & t \leq t_0, \\ e^{-it\hat{H}}|_{\kappa=\kappa_2} |\psi_0\rangle, & t \geq t_0, \end{cases} \quad (6.2)$$

where $\kappa_{1,2}$ indicates different values for κ in (2.10). One could study first and second-order phase transitions in the BBJM model under the local quench above using an appropriate order parameter, such as κ in (2.10). This could allow us to study evolution of real time thermal correlation (2.21) and the free energy corresponding to the on-shell action (2.16) in the quenched systems. There are different examples in condensed matter (see e.g. [120–123]) and holographic (see e.g. [124–126]) systems where local quenches may alter macroscopic properties of the system that are similar to those in hysteresis where the properties of the system depend on its past history. It would be interesting to investigate if (6.2) indeed results in these effects in the corresponding phase transition.

Multiple flavored chord Hamiltonians It might be interesting to extend our study about dynamical probes of chaos for more general types of chord Hamiltonian systems (relevant discussions have been raised in [23, 25]), where instead of two systems one includes arbitrarily many (see App. A.5). In particular, the double-scaling limit of the commuting SYK model [41] with multiple types (which we refer to as “flavors”) of chords was developed in [25]. In this case, the condition $q_{ij} = q \forall i, j \in \mathbb{N}$ is automatically imposed in the setup, which allows to study the collective chaotic behaviour of multiple double-scaled “integrable” SYKs and its thermodynamics. This would be a very convenient setting to further investigate the construction of the Krylov basis for spread complexity in Sec. 3 where the condition $q_{ij} = q$ leads to analytically solvable expressions. This may allow us to further develop our study of Krylov operator complexity based on the two-point functions (Sec. 4) using the results in [25]. This could extend our study of the integrable-chaotic phase transition in a chord diagram Hamiltonian with multiple (integrable) fields. We hope to report on new findings regarding this direction in the future.

Acknowledgments

We thank Marco Ambrosini, Micha Berkooz, Andreas Blommaert and Saskia Demulder for useful discussions. We are indebted to the organizers of the Joint Belgian hep-th seminars at Université Libre de Bruxelles; the YITP-I-25-01 “Black Hole, Quantum Chaos and Quantum Information” workshop at Yukawa Institute for Theoretical Physics, Kyoto University; “QIQQ 2025: Quantum Information In Quantum Gravity” at Perimeter Institute and “2025 East Asia Joint Workshop on Fields and Strings” at Okinawa Institute of Science and Technology where this work was developed at different stages; and “Gravity meets quantum information” at Würzburg University, which allowed this collaboration to start. SEAG thanks

the High Energy Physics group in UC Santa Barbara and Rikkyo University for hosting him during different stages of this manuscript, and for travel support from the QISS consortium, and the YITP. SEAG is supported by the Okinawa Institute of Science and Technology Graduate University. This work was made possible through the support of the WOST, WithOut SpaceTime project (<https://withoutspacetime.org>), supported by Grant ID# 63683 from the John Templeton Foundation (JTF). The opinions expressed in this work are those of the author(s) and do not necessarily reflect the views of the John Templeton Foundation. RND's work leading to this publication was supported by the PRIME programme of the German Academic Exchange Service (DAAD) with funds from the German Federal Ministry of Research, Technology and Space (BMFTR). RND and JE are also supported by Germany's Excellence Strategy through the Würzburg-Dresden Cluster of Excellence on Complexity, Topology and Dynamics in Quantum Matter - ctd.qmat (EXC 2147, project-id 390858490). ZYX also acknowledges support from the Berlin Quantum Initiative.

A Supplementary Background Material

In this appendix we provide complementary background to Sec. 2,. We explain about the definitions of the chaos measures used in the main text, including Krylov state (spread) complexity (App. A.1), Krylov operator complexity (App. A.2), OTOCs at finite temperatures (App. A.3); basics on the DSSYK model, as well as the commuting DSSYK model (App. A.4), which is a specific realization of the integrable model \hat{H}_2 in (1.1); and the multifield formalism for multiple ensemble-averaged double-scaled model (App. A.5).

A.1 Krylov state (spread) complexity

Starting from the Schrödinger picture for a generic pure quantum system, we would like to construct an ordered, orthonormal basis of states $\{|B_n\rangle\}$ that minimizes

$$\sum_n c_n |\langle \phi(t) | |B_n\rangle|^2$$

where c_n is an arbitrary monotonically increasing real sequence, and

$$|\phi(t)\rangle = e^{-iHt} |\phi_0\rangle. \quad (\text{A.1})$$

It was found in [8] that the solution to this problem is the so-called Krylov basis, $|K_n\rangle$, defined through the Lanczos algorithm shown below

$$|A_{n+1}\rangle \equiv (\hat{H} - a_n) |K_n\rangle - b_n |K_{n-1}\rangle, \quad (\text{A.2})$$

$$|K_n\rangle \equiv b_n^{-1} |A_n\rangle. \quad (\text{A.3})$$

Here $|K_0\rangle \equiv |\phi_0\rangle$ and

$$a_n \equiv \langle K_n | \hat{H} | K_n \rangle, \quad b_n \equiv (\langle A_n | A_n \rangle)^{1/2}, \quad (\text{A.4})$$

are called the Lanczos coefficients. Using this basis, $|\phi(t)\rangle$ can be expressed as

$$|\phi(t)\rangle = \sum_{n=0}^{\mathcal{K}} \phi_n(t) |K_n\rangle. \quad (\text{A.5})$$

Here \mathcal{K} denotes the Krylov space dimension, which satisfies $\mathcal{K} \leq \dim(\mathcal{H})$. The Hamiltonian in this basis becomes tridiagonal, and we can express a recursive relation between the time-dependent components in (A.5) as a Schrödinger equation:

$$i\partial_t \phi_n(t) = a_n \phi_n(t) + b_{n+1} \phi_{n+1}(t) + b_n \phi_{n-1}(t), \quad (\text{A.6})$$

with $\sum_n |\phi_n(t)|^2 = 1$. Krylov complexity for states (also called spread complexity) can be defined as

$$C_S(t) \equiv \sum_n f(n) |\phi_n(t)|^2, \quad (\text{A.7})$$

where $f(n)$ is a monotonically increasing sequence in terms of n . In the main text, we set $f(n) = n$, so that spread complexity represents a position expectation value in an ordered lattice given by the Krylov basis $|K_n\rangle$.

Intuitively, C_S measures the average position in a one-dimensional chain generated by the Krylov basis, where each step along the chain represents an increasingly chaotic state since they roughly behave as $|K_n\rangle \approx \hat{H}^n |\phi_0\rangle$.

A.2 Krylov operator complexity

Consider an operator \hat{O} in the Heisenberg picture. We would like to express it in terms of a complete and ordered basis of states $\{|\chi_n\rangle\}$ as

$$|\hat{O}\rangle \equiv \sum_{m,n} O_{nm} |\chi_m, \chi_n\rangle, \quad (\text{A.8})$$

where $O_{nm} \equiv \langle \chi_m | \hat{O} | \chi_n \rangle$. Given the thermal ensemble describing the DSSYK model, we will define the Frobenius inner product (while for thermal ensembles one needs to modify the definition, see e.g. [7, 101, 127]):

$$(X|Y) = \frac{1}{Z(\beta)} \text{tr}(e^{-\frac{\beta}{2}\hat{H}} \hat{X}^\dagger e^{-\frac{\beta}{2}\hat{H}} \hat{Y}). \quad (\text{A.9})$$

We can represent the evolution of the operator through the Heisenberg equation as

$$\partial_t |\hat{O}(t)\rangle = i\hat{\mathcal{L}} |\hat{O}(t)\rangle, \quad (\text{A.10})$$

where \mathcal{L} is called the Liouvillian super-operator,

$$\hat{\mathcal{L}} = [\hat{H}, \cdot], \quad \hat{O}(t) = e^{i\hat{\mathcal{L}}t} \hat{O}. \quad (\text{A.11})$$

We can then solve (A.10) in terms of a Krylov basis, $\{|O_n\rangle\}$,

$$\begin{aligned} |O(t)\rangle &= \sum_{n=0}^{\mathcal{K}-1} i^n \varphi_n(t) |O_n\rangle, \\ \varphi_n(t) &= (O_n | e^{i\hat{\mathcal{L}}t} | O_n \rangle, \quad (O_m | O_n \rangle = \delta_{mn}. \end{aligned} \quad (\text{A.12})$$

Moreover, assuming that $\hat{O}(t)$ is a Hermitian operator, the correlation function is an even function in t that can be expanded as a Taylor series as

$$\varphi_0(t) = (O(t)|O(0)) = \sum_n m_{2n} \frac{(-1)^n t^{2n}}{(2n)!}, \quad (\text{A.13})$$

where m_{2n} are referred to as the moments. It follows that given an autocorrelation function ($\varphi_0(t)$), the moments are easily accessed from

$$m_{2n} = (-1)^n \left(\frac{d}{dt} \right)^{2n} \varphi_0(t) \Big|_{t=0}. \quad (\text{A.14})$$

The Lanczos coefficients b_n can be then determined from the moments using an algorithm [7, 128, 129]

$$b_n = \sqrt{Q_{2n}^{(n)}}, \quad Q_{2k}^{(m)} = \frac{Q_{2k}^{(m-1)}}{b_{m-1}^2} - \frac{Q_{2k-2}^{(m-2)}}{b_{m-2}^2}, \quad (\text{A.15})$$

where $Q_{2k}^{(0)} = m_{2k}$, and $Q_{2k}^{(-1)} = 0$.

The other amplitudes can be determined through the Lanczos algorithm and the Heisenberg equation (A.10), leading to the recursion relation:

$$\partial_t \varphi_n(t) = b_n \varphi_{n-1}(t) - b_{n+1} \varphi_{n+1}(t). \quad (\text{A.16})$$

Krylov operator complexity is then defined as

$$\mathcal{C}_K(t) \equiv \sum_{n=0}^{K-1} n |\varphi_n(t)|^2. \quad (\text{A.17})$$

The definition above was originally motivated [7] to describe the size of the operator under Hamiltonian evolution, as it measures the mean width of a wavepacket in the Krylov space.

A.3 OTOCs at finite temperature

In connection to Sec. 5, we now review how to carry out the evaluation of crossed four point functions at finite temperature in the SYK model, based on the [105, 106].

In the DSSYK model, a semiclassical approximation for OTOCs away from the triple-scaling limit was derived in [38, 40] (see also e.g. [37, 53]), while the triple scaling limit (i.e. the low-energy regime) result had been obtained in previous works [27, 130].

However, once we incorporate integrable and chaotic chords, the procedure above requires further adjustments. We choose to approach this problem with from the generating function of general fermionic correlation functions at finite temperature (first illustrated in [105, 106]), and then take the double-scaling limit of the results. For this reason we begin with the $2n$ -point generating function

$$Z_\mu[\rho^{1/2}] = \left\langle \rho^{1/2} \Big| e^{-\mu \hat{s}} \Big| \rho^{1/2} \right\rangle, \quad (\text{A.18})$$

where the factor $e^{-\mu\hat{s}}$ generates Euclidean evolution. The crossed four-point function of interest is

$$\mathcal{G}_\mu(\tau_a, \tau_b) = \frac{\langle 0 | \mathcal{T} e^{-\frac{\beta}{2}(\hat{H}_L + \hat{H}_R)} e^{-\mu\hat{s}\left(\frac{\beta}{4}\right)} \psi_1^L(\tau_a) \psi_1^L(\tau_b) | 0 \rangle}{\langle 0 | \mathcal{T} e^{-\frac{\beta}{2}(\hat{H}_L + \hat{H}_R)} e^{-\mu n\left(\frac{\beta}{4}\right)} | 0 \rangle}. \quad (\text{A.19})$$

where \hat{s} is the size operator

$$\hat{s} = -\frac{i}{2} \sum_{j=1}^N \psi_j^L \psi_j^R. \quad (\text{A.20})$$

We can see that $\mathcal{G}_{\mu=0}$ gives a two-point function, while the OTOC can be computed from $-\lim_{\mu \rightarrow 0} \partial_\mu \mathcal{G}_\mu$. This can be more conveniently evaluated using

$$e^{\mu n} \begin{pmatrix} \psi_L \\ i\psi_R \end{pmatrix} e^{-\mu n} = \begin{pmatrix} \cosh \mu & -\sinh \mu \\ -\sinh \mu & \cosh \mu \end{pmatrix} \begin{pmatrix} \psi_L \\ i\psi_R \end{pmatrix}, \quad (\text{A.21})$$

which can be expressed in terms of a single field ψ defined as

$$\psi_i(\tau) = \begin{cases} \psi_L(\tau), & 0 < \tau < \beta/2, \\ \psi_R(\beta - \tau), & \beta/2 < \tau < \beta, \end{cases} \quad (\text{A.22})$$

where we impose twisted boundary conditions, defined by

$$\psi(\tau) = -\psi(\tau + \beta), \quad (\text{A.23})$$

so that (A.21) can be expressed

$$\lim_{\mu \rightarrow \beta/4^+} e^{\mu n} \begin{pmatrix} \psi(\tau) \\ \psi(\beta - \tau) \end{pmatrix} e^{-\mu n} = \lim_{\mu \rightarrow \beta/4^-} \begin{pmatrix} \cosh \mu & -\sinh \mu \\ -\sinh \mu & \cosh \mu \end{pmatrix} \begin{pmatrix} \psi(\tau) \\ \psi(\beta - \tau) \end{pmatrix}. \quad (\text{A.24})$$

The role of (A.23) is to generate the crossing between the fermions in the OTOC.

We note that (A.24) can be evaluated from (A.18) as

$$\mathcal{G}_\mu(\hat{\mathcal{O}}_\Delta) = \frac{Z_\mu[\hat{\mathcal{O}}_\Delta \rho^{1/2}]}{Z_\mu[\rho^{1/2}]}, \quad (\text{A.25})$$

when $\hat{\mathcal{O}}_\Delta = \psi_1(t) \rho^{1/2}$. This calculation can be expanded in terms of twisted boundary conditions:

$$\begin{pmatrix} \lim_{\tau_{1/2} \rightarrow \beta/4^+} \mathcal{G}_\mu(\tau_1, \tau_2) \\ \lim_{\tau_{1/2} \rightarrow \beta/4^-} \mathcal{G}_\mu(\tau_1, \tau_2) \end{pmatrix} = \begin{pmatrix} \cosh \mu & -\sinh \mu \\ -\sinh \mu & \cosh \mu \end{pmatrix} \begin{pmatrix} \lim_{\tau_{1/2} \rightarrow \beta/4^-} \mathcal{G}_\mu(\tau_1, \tau_2) \\ \lim_{\tau_{1/2} \rightarrow \beta/4^+} \mathcal{G}_\mu(\tau_1, \tau_2) \end{pmatrix}. \quad (\text{A.26})$$

\mathcal{G}_μ can then be solved in terms of a fundamental domain where $0 < \tau_1 - \tau_2 < \beta/2$. In our notation, when p is fixed, and $N \gg 1$, one can analytically recover the two-point functions and OTOCs [105]. We implement this in Sec. 5 for the integrable-chaotic chord Hamiltonian model.

A.4 The Double-Scaled SYK and Commuting SYK Models

We presented the physical SYK origins of the model in Sec. 2.1, we now describe its auxiliary Hilbert space in more detail. As reviewed e.g. [28], one can construct an orthonormal basis (i.e. $\langle n | m \rangle = \delta_{nm}$), to write the Hamiltonian of the auxiliary system in the form

$$\hat{H}_1 = \frac{J}{\sqrt{\lambda}} (\hat{a}_n + \hat{a}_n^\dagger), \quad (\text{A.27})$$

where \hat{a}_n and \hat{a}_n^\dagger are creation and annihilation operators acting on the $\{|n\rangle\}$ basis,

$$\hat{a}_n |n\rangle = \sqrt{[n]_q} |n-1\rangle, \quad \hat{a}_n^\dagger |n\rangle = \sqrt{[n+1]_q} |n+1\rangle, \quad [n]_q \equiv \frac{1-q^n}{1-q}. \quad (\text{A.28})$$

We also introduce matter chord operators in this model

$$V := \sum_{I'} J_{I'} \Psi_{I'}, \quad (\text{A.29})$$

where, similarly to (2.1), I' is a collective indicating $1 \leq i_1 \leq i_2 \leq \dots \leq i_{p'} \leq N$, where $\Delta := p'/p$ is associated as the conformal dimension of the operator [27], and $J_{I'} := J_{i_1, \dots, i_{p'}}$.

It has been noticed that the chord number basis of the DSSYK model forms a Krylov basis [107], so that $|K_n\rangle = |n\rangle$, and the spread complexity for this model has been calculated in the natural TFD state $e^{-it\hat{H}_1} |0\rangle$ by [77]. The analytic expression was generalized including finite temperature effects by considering the Krylov complexity of the Hartle-Hawking state in the semiclassical regime of the DSSYK model

$$\lim_{\lambda \rightarrow 0} C_S(t) = \frac{2}{\lambda} \log \frac{\cosh(2\mathcal{J} \sin \theta t)}{\sin \theta}, \quad (\text{A.30})$$

where θ parametrizes the energy of the DSSYK model

$$E(\theta) = \frac{2\mathcal{J}}{\sqrt{\lambda(1-q)}} \cos \theta. \quad (\text{A.31})$$

Further generalizations in Krylov complexity/wormhole length dictionary have been reported with matter contributions [38–40, 103], supersymmetry [80], conserved charges [131], and finite N effects [79, 132, 133].

Commuting DSSYK model Similarly, for the commuting SYK (2.4) in the double scaling limit has a span of states $\{|z\rangle\}$ are described with a Hamiltonian

$$\hat{H}_2 = J(\hat{a}_z + \hat{a}_z^\dagger), \quad (\text{A.32})$$

which now obeys a Heisenberg-Weyl algebra $[a_z, a_z^\dagger]_1 = 1$.

As in the previous subsection, we will consider the Krylov complexity as the expectation value of the chord number operator \hat{s} for the infinite-temperature TFD state $e^{-it\hat{H}_{\text{com}}} |0\rangle$,

where \hat{H}_{com} is the chord Hamiltonian \hat{H}_2 in (2.4). The result has been computed for us by [24] (see their (2.15), which is at finite temperature),

$$\mathcal{C}_S(t) = \frac{\mathcal{J}^2}{2} \left(t^2 + \frac{\beta^2}{4} \right). \quad (\text{A.33})$$

We also know the OTOC [24] (3.8)

$$\begin{aligned} & \frac{1}{Z} \text{tr} [\text{e}^{-\beta H} [W(0), V(t)]^2] \\ &= -2 + 2 \cos \left[(1 - e^{-\Delta_V}) (1 - e^{-\Delta_W}) J^2 \beta t / 2 \right] e^{-\Delta_V \Delta_W - (1 - e^{-\Delta_V}) (1 - e^{-\Delta_W}) J^2 t^2}, \end{aligned} \quad (\text{A.34})$$

where $W(t)$ and $V(0)$ are matter operators (A.29) with conformal weight Δ_V and Δ_W respectively.

Moreover, given that the integrable model is described by a quantum harmonic oscillator Hamiltonian, the Krylov complexity for integrable matter operators V (A.29) with a conformal weight Δ becomes (see the Heisenberg-Weyl algebra case in [99])

$$\mathcal{C}_O(t) = 2\Delta(\mathcal{J}\kappa t)^2. \quad (\text{A.35})$$

A.5 Multifield Liouville formulation

One can build other generalizations of the above double-scaled DSSYK model and its integrable counterpart, which are conveniently treated in the multifield formalism in [23]; valid for arbitrarily many types of chords. The starting point in this formalism is the theory

$$\hat{H} = \sum_{i=1}^K \kappa_i^2 \hat{H}_i, \quad (\text{A.36})$$

where each \hat{H}_i is a random Hamiltonian in the same universality class as the original DSSYK model [26, 27], and the chord crossing weight between Hamiltonians \hat{H}_i and \hat{H}_j is denoted $q^{\alpha_{ij}}$; κ_i are numerical coefficients that we take to satisfy a convenient normalization

$$\sum_{i=1}^K |\kappa_i|^2 = 1, \quad (\text{A.37})$$

and K is the total number of random Hamiltonians. The partition function in this theory can be expressed

$$\int \left(\prod_{i=1}^K \mathcal{D}[g_i] \right) \exp \left[\frac{1}{\lambda} \iint_0^\beta d\tau_1 d\tau_2 \left[\sum_{i,j=1}^K \alpha_{ij} g_i \partial_1 \partial_2 g_j + 4\mathcal{J}^2 \sum_{i=1}^K \kappa_i^2 e^{\sum_j \alpha_{ij} g_j} \right] \right], \quad (\text{A.38})$$

where α_{ij} is a set of constants. The two-chord Hamiltonian system corresponds to

$$\alpha_{ij} = \begin{pmatrix} 1 & \Delta \\ \Delta & \alpha' \end{pmatrix}. \quad (\text{A.39})$$

The integrable deformation of the DSSYK model (1.1) is then $\alpha' = 0$; which is a case of interest for us.

B More details about (2.8)

In this appendix, we study whether (2.8) can be used as a Krylov basis for the Hamiltonian (2.10). We consider the following infinite-temperature TFD state [77, 107] as a reference state

$$|\phi(t)\rangle := e^{-i\hat{H}t} |0\rangle = \sum_{n,z} \phi_{n,z}(t) |n, z; \vec{r}\rangle, \quad (\text{B.1})$$

where we have assumed $\{|n, z; \vec{r}\rangle\}$ is a complete basis; and we defined $\phi_{n,z} := \langle\langle n, z; \vec{r}| e^{-i\hat{H}t} |0\rangle\rangle$. Acting with the creation/annihilation operators in (2.10) on the above state results in

$$\begin{aligned} \hat{H} |\phi(t)\rangle &= \nu \sum_{n,z} \left[\sqrt{[n+1]_{q_n}} \phi_{n+1,z} |n, z; \vec{r}_1\rangle + \sqrt{[n]_{q_n}} \phi_{n-1,z} |n, z; \vec{r}_2\rangle \right] \\ &\quad + \kappa \sum_{n,z} \left[\sqrt{[z+1]_{q_z}} \phi_{n,z+1} |n, z; \vec{r}_3\rangle + \sqrt{[z]_{q_z}} \phi_{n,z-1} |n, z; \vec{r}_4\rangle \right], \end{aligned} \quad (\text{B.2})$$

where, given that the vectors \vec{r}_i are manifestly different from each other (due to the different applications of \hat{a}_i), the basis $\{|n, z; \vec{r}\rangle\}$ even if complete, is not a Krylov basis in the sense of the Lanczos algorithm (see (A.6)). For this reason, we focused on the special case $q_{nn} = q_{zz} = q_{nz}$ in the main text.

C Deviations from the $q_{nn} = q_{nz} = q_{zz}$ Krylov basis

In this appendix we complete our discussion of Sec. 3.1 regarding corrections to the Krylov basis away from the case where the Hamiltonian crossings are $q_{nn} = q_{nz} = q_{zz}$.

We begin considering small derivations from $|q_{nn} - q_{nz}| \sim |q_{nz} - q_{zz}| \sim dz \ll 1$ and we denote the total Hamiltonian with a deviation d as H_d . From (3.9) we identify

$$\delta b_n^2 = \frac{n(n-1)}{2} d. \quad (\text{C.1})$$

The variation of μ_{2n} can also be evaluated from (C.1) and (3.10) as

$$\ln \mu_{2n} = \sum_{m=1}^n \ln b_m^2, \quad \delta \mu_{2n} = \mu_{2n} \sum_{m=1}^n \frac{\delta b_m^2}{b_m^2} = \mu_{2n} d \sum_{m=1}^n \frac{m(m-1)}{2 b_m^2}. \quad (\text{C.2})$$

Next, we define the error state

$$|\mathcal{E}_{n+1}\rangle := H_d |P_n\rangle - b_n^2 |P_{n-1}\rangle - b_{n+1} |P_{n+1}\rangle, \quad (\text{C.3})$$

where $|P_k\rangle$ is taken as (3.9). The relative error can then be expressed as

$$\frac{\langle \mathcal{E}_{n+1} | \mathcal{E}_{n+1} \rangle}{\langle P_{n+1} | P_{n+1} \rangle} = \frac{\langle P_n | (H_d - H_0)^2 | P_n \rangle}{\langle P_n | P_n \rangle b_{n+1}^2}. \quad (\text{C.4})$$

This indicates the degree to which we can approximately describe the system away from $q_{nn} = q_{nz} = q_{zz}$ with the same Krylov basis in Sec. 3.2.

References

- [1] I. Aleiner and A. Larkin, *Divergence of classical trajectories and weak localization*, *Physical Review B* **54** (1996) 14423.
- [2] E.B. Rozenbaum, S. Ganeshan and V. Galitski, *Lyapunov Exponent and Out-of-Time-Ordered Correlator's Growth Rate in a Chaotic System*, *Phys. Rev. Lett.* **118** (2017) 086801 [[1609.01707](#)].
- [3] J.S. Cotler, G. Gur-Ari, M. Hanada, J. Polchinski, P. Saad, S.H. Shenker et al., *Black Holes and Random Matrices*, *JHEP* **05** (2017) 118 [[1611.04650](#)].
- [4] F.J. Dyson, *Statistical theory of the energy levels of complex systems. I*, *J. Math. Phys.* **3** (1962) 140.
- [5] F.J. Dyson, *Statistical Theory of the Energy Levels of Complex Systems. III*, *J. Math. Phys.* **3** (1962) 166.
- [6] E.P. Wigner, *Characteristic vectors of bordered matrices with infinite dimensions i*, *The Collected Works of Eugene Paul Wigner: Part A: The Scientific Papers* (1993) 524.
- [7] D.E. Parker, X. Cao, A. Avdoshkin, T. Scaffidi and E. Altman, *A Universal Operator Growth Hypothesis*, *Phys. Rev. X* **9** (2019) 041017 [[1812.08657](#)].
- [8] V. Balasubramanian, P. Caputa, J.M. Magan and Q. Wu, *Quantum chaos and the complexity of spread of states*, *Phys. Rev. D* **106** (2022) 046007 [[2202.06957](#)].
- [9] J. Erdmenger, S.-K. Jian and Z.-Y. Xian, *Universal chaotic dynamics from Krylov space*, *JHEP* **08** (2023) 176 [[2303.12151](#)].
- [10] E. Rabinovici, A. Sánchez-Garrido, R. Shir and J. Sonner, *Krylov Complexity*, [2507.06286](#).
- [11] S. Baiguera, V. Balasubramanian, P. Caputa, S. Chapman, J. Haferkamp, M.P. Heller et al., *Quantum complexity in gravity, quantum field theory, and quantum information science*, [2503.10753](#).
- [12] P. Nandy, A.S. Matsoukas-Roubeas, P. Martínez-Azcona, A. Dymarsky and A. del Campo, *Quantum dynamics in Krylov space: Methods and applications*, *Phys. Rept.* **1125-1128** (2025) 1 [[2405.09628](#)].
- [13] V. Balasubramanian, R.N. Das, J. Erdmenger and Z.-Y. Xian, *Chaos and integrability in triangular billiards*, *J. Stat. Mech.* **2025** (2025) 033202 [[2407.11114](#)].
- [14] H.A. Camargo, K.-B. Huh, V. Jahnke, H.-S. Jeong, K.-Y. Kim and M. Nishida, *Spread and spectral complexity in quantum spin chains: from integrability to chaos*, *JHEP* **08** (2024) 241 [[2405.11254](#)].
- [15] E. Rabinovici, A. Sánchez-Garrido, R. Shir and J. Sonner, *Krylov complexity from integrability to chaos*, *JHEP* **07** (2022) 151 [[2207.07701](#)].
- [16] M. Alishahiha, S. Banerjee and M.J. Vasli, *Krylov complexity as a probe for chaos*, *Eur. Phys. J. C* **85** (2025) 749 [[2408.10194](#)].
- [17] E. Rabinovici, A. Sánchez-Garrido, R. Shir and J. Sonner, *Krylov localization and suppression of complexity*, *JHEP* **03** (2022) 211 [[2112.12128](#)].

- [18] M. Baggioli, K.-B. Huh, H.-S. Jeong, K.-Y. Kim and J.F. Pedraza, *Krylov complexity as an order parameter for quantum chaotic-integrable transitions*, [2407.17054](#).
- [19] G.F. Scialchi, A.J. Roncaglia and D.A. Wisniacki, *Integrability-to-chaos transition through the Krylov approach for state evolution*, *Phys. Rev. E* **109** (2024) 054209 [[2309.13427](#)].
- [20] B. Bhattacharjee and P. Nandy, *Krylov fractality and complexity in generic random matrix ensembles*, *Phys. Rev. B* **111** (2025) L060202 [[2407.07399](#)].
- [21] M. Berkooz, N. Brukner, Y. Jia and O. Mamroud, *A Path Integral for Chord Diagrams and Chaotic-Integrable Transitions in Double Scaled SYK*, [2403.05980](#).
- [22] M. Berkooz, N. Brukner, Y. Jia and O. Mamroud, *From Chaos to Integrability in Double Scaled SYK*, [2403.01950](#).
- [23] M. Berkooz, R. Frumkin, O. Mamroud and J. Seitz, *Twisted times, the Schwarzian and its deformations in DSSYK*, [2412.14238](#).
- [24] A. Almheiri, A. Goel and X.-Y. Hu, *Quantum gravity of the Heisenberg algebra*, [2403.18333](#).
- [25] P. Gao, H. Lin and C. Peng, *D-commuting SYK model: building quantum chaos from integrable blocks*, [2411.12806](#).
- [26] M. Berkooz, P. Narayan and J. Simon, *Chord diagrams, exact correlators in spin glasses and black hole bulk reconstruction*, *JHEP* **08** (2018) 192 [[1806.04380](#)].
- [27] M. Berkooz, M. Isachenkov, V. Narovlansky and G. Torrents, *Towards a full solution of the large N double-scaled SYK model*, *JHEP* **03** (2019) 079 [[1811.02584](#)].
- [28] M. Berkooz and O. Mamroud, *A Cordial Introduction to Double Scaled SYK*, [2407.09396](#).
- [29] M. Berkooz, M. Isachenkov, M. Isachenkov, P. Narayan and V. Narovlansky, *Quantum groups, non-commutative AdS_2 , and chords in the double-scaled SYK model*, *JHEP* **08** (2023) 076 [[2212.13668](#)].
- [30] A. Blommaert, T.G. Mertens and S. Yao, *Dynamical actions and q -representation theory for double-scaled SYK*, *JHEP* **02** (2024) 067 [[2306.00941](#)].
- [31] A. Almheiri and F.K. Popov, *Holography on the quantum disk*, *JHEP* **06** (2024) 070 [[2401.05575](#)].
- [32] A. Belaey, T.G. Mertens and T. Tappeiner, *Quantum group origins of edge states in double-scaled SYK*, [2503.20691](#).
- [33] J. van der Heijden, E. Verlinde and J. Xu, *Quantum Symmetry and Geometry in Double-Scaled SYK*, [2511.08743](#).
- [34] K. Schouten and M. Isachenkov, *The von Neumann algebraic quantum group $SU_q(1,1) \rtimes \mathbb{Z}_2$ and the DSSYK model*, [2512.10101](#).
- [35] J. Xu, *Von Neumann Algebras in Double-Scaled SYK*, [2403.09021](#).
- [36] X. Cao and P. Gao, *Single-Sided Black Holes in Double-Scaled SYK Model and No Man's Island*, [2511.01978](#).
- [37] H.W. Lin and D. Stanford, *A symmetry algebra in double-scaled SYK*, *SciPost Phys.* **15** (2023) 234 [[2307.15725](#)].

[38] S.E. Aguilar-Gutierrez, *Building the Holographic Dictionary of the DSSYK from Chords, Complexity & Wormholes with Matter*, [2505.22716](#).

[39] J. Xu, *On chord dynamics and complexity growth in double-scaled SYK*, [JHEP 06 \(2025\) 259](#) [[2411.04251](#)].

[40] S.E. Aguilar-Gutierrez and J. Xu, *Geometry of Chord Intertwiner, Multiple Shocks and Switchback in Double-Scaled SYK*, [2506.19013](#).

[41] P. Gao, *Commuting SYK: a pseudo-holographic model*, [JHEP 01 \(2024\) 149](#) [[2306.14988](#)].

[42] D. Jafferis, A. Zlokapa, J.D. Lykken, D.K. Kolchmeyer, S.I. Davis, N. Lauk et al., *Traversable wormhole dynamics on a quantum processor*, [Nature 612 \(2022\) 51](#).

[43] A. Blommaert, T.G. Mertens and J. Papalini, *The dilaton gravity hologram of double-scaled SYK*, [2404.03535](#).

[44] A. Blommaert, A. Levine, T.G. Mertens, J. Papalini and K. Parmentier, *An entropic puzzle in periodic dilaton gravity and DSSYK*, [JHEP 07 \(2025\) 093](#) [[2411.16922](#)].

[45] A. Blommaert, A. Levine, T.G. Mertens, J. Papalini and K. Parmentier, *Wormholes, branes and finite matrices in sine dilaton gravity*, [JHEP 09 \(2025\) 123](#) [[2501.17091](#)].

[46] A. Blommaert and A. Levine, *Sphere amplitudes and observing the universe's size*, [2505.24633](#).

[47] L. Bossi, L. Griguolo, J. Papalini, L. Russo and D. Seminara, *Sine-dilaton gravity vs double-scaled SYK: exploring one-loop quantum corrections*, [JHEP 06 \(2025\) 152](#) [[2411.15957](#)].

[48] A. Blommaert, D. Tietto and H. Verlinde, *SYK collective field theory as complex Liouville gravity*, [2509.18462](#).

[49] C. Cui and M. Rozali, *Splitting and gluing in sine-dilaton gravity: matter correlators and the wormhole Hilbert space*, [2509.01680](#).

[50] V. Narovlansky and H. Verlinde, *Double-scaled SYK and de Sitter holography*, [JHEP 05 \(2025\) 032](#) [[2310.16994](#)].

[51] H. Verlinde, *Double-scaled SYK, chords and de Sitter gravity*, [JHEP 03 \(2025\) 076](#) [[2402.00635](#)].

[52] H. Verlinde and M. Zhang, *SYK correlators from 2D Liouville-de Sitter gravity*, [JHEP 05 \(2025\) 053](#) [[2402.02584](#)].

[53] V. Narovlansky, *Towards a microscopic description of de Sitter dynamics*, [2506.02109](#).

[54] H. Verlinde, *Talks given at the QGQC5 conference, UC Davis; the Franqui Symposium, Brussels; ‘Quantum Gravity on Southern Cone’, Argentina; and ‘SYK models and Gauge Theory’ workshop at Weizmann Institute*, 2019.

[55] S.E. Aguilar-Gutierrez, *Towards complexity in de Sitter space from the double-scaled Sachdev-Ye-Kitaev model*, [JHEP 10 \(2024\) 107](#) [[2403.13186](#)].

[56] R. Jackiw, *Lower dimensional gravity*, [Nuclear Physics B 252 \(1985\) 343](#).

[57] C. Teitelboim, *Gravitation and hamiltonian structure in two spacetime dimensions*, [Physics Letters B 126 \(1983\) 41](#).

- [58] L. Susskind, *Entanglement and Chaos in De Sitter Space Holography: An SYK Example*, *JHAP* **1** (2021) 1 [[2109.14104](#)].
- [59] L. Susskind, *De Sitter Space, Double-Scaled SYK, and the Separation of Scales in the Semiclassical Limit*, *JHAP* **5** (2025) 1 [[2209.09999](#)].
- [60] L. Susskind, *De Sitter Space has no Chords. Almost Everything is Confined.*, *JHAP* **3** (2023) 1 [[2303.00792](#)].
- [61] H. Lin and L. Susskind, *Infinite Temperature's Not So Hot*, [2206.01083](#).
- [62] A.A. Rahman, *dS JT Gravity and Double-Scaled SYK*, [2209.09997](#).
- [63] A.A. Rahman and L. Susskind, *Comments on a Paper by Narovlansky and Verlinde*, [2312.04097](#).
- [64] A.A. Rahman and L. Susskind, *p-Chords, Wee-Chords, and de Sitter Space*, [2407.12988](#).
- [65] A. Rahman and L. Susskind, *Infinite Temperature is Not So Infinite: The Many Temperatures of de Sitter Space*, [2401.08555](#).
- [66] Y. Sekino and L. Susskind, *Double-Scaled SYK, QCD, and the Flat Space Limit of de Sitter Space*, [2501.09423](#).
- [67] S. Miyashita, Y. Sekino and L. Susskind, *DSSYK at Infinite Temperature: The Flat-Space Limit and the 't Hooft Model*, [2506.18054](#).
- [68] D. Tietto and H. Verlinde, *A microscopic model of de Sitter spacetime with an observer*, [2502.03869](#).
- [69] A. Milekhin and J. Xu, *Revisiting Brownian SYK and its possible relations to de Sitter*, *JHEP* **10** (2024) 151 [[2312.03623](#)].
- [70] K. Okuyama, *De Sitter JT gravity from double-scaled SYK*, [2505.08116](#).
- [71] H. Yuan, X.-H. Ge and K.-Y. Kim, *Pole skipping in two-dimensional de Sitter spacetime and double-scaled SYK model*, *Phys. Rev. D* **112** (2025) 026022 [[2408.12330](#)].
- [72] D. Gaiotto and H. Verlinde, *SYK-Schur duality: double scaled SYK correlators from $\mathcal{N} = 2$ supersymmetric gauge theory*, *JHEP* **06** (2025) 163 [[2409.11551](#)].
- [73] S.E. Aguilar-Gutierrez, *Symmetry Sectors in Chord Space and Relational Holography in the DSSYK*, [2506.21447](#).
- [74] S.E. Aguilar-Gutierrez, *T^2 deformations in the double-scaled SYK model: Stretched horizon thermodynamics*, [2410.18303](#).
- [75] S.E. Aguilar-Gutierrez, *Cosmological Entanglement Entropy and Edge Modes from Double-Scaled SYK & Its Connection with Krylov Complexity*, [2511.03779](#).
- [76] M.P. Heller, F. Ori, J. Papalini, T. Schuhmann and M.-T. Wang, *De Sitter holographic complexity from Krylov complexity in DSSYK*, [2510.13986](#).
- [77] E. Rabinovici, A. Sánchez-Garrido, R. Shir and J. Sonner, *A bulk manifestation of Krylov complexity*, *JHEP* **08** (2023) 213 [[2305.04355](#)].
- [78] M.P. Heller, J. Papalini and T. Schuhmann, *Krylov spread complexity as holographic complexity beyond JT gravity*, [2412.17785](#).

[79] V. Balasubramanian, J.M. Magan, P. Nandi and Q. Wu, *Spread complexity and the saturation of wormhole size*, [2412.02038](#).

[80] S.E. Aguilar-Gutierrez, *Evolution With(out) Time: Relational Holography & BPS Complexity Growth in $\mathcal{N} = 2$ Double-Scaled SYK*, [2510.11777](#).

[81] A. Chamblin, R. Emparan, C.V. Johnson and R.C. Myers, *Charged AdS black holes and catastrophic holography*, *Phys. Rev. D* **60** (1999) 064018 [[hep-th/9902170](#)].

[82] A. Chamblin, R. Emparan, C.V. Johnson and R.C. Myers, *Holography, thermodynamics and fluctuations of charged AdS black holes*, *Phys. Rev. D* **60** (1999) 104026 [[hep-th/9904197](#)].

[83] M.B. Awal and P. Phukon, *Probing thermodynamic phase transitions of 4D R-charged black holes via lyapunov exponent*, *Nucl. Phys. B* **1021** (2025) 117176 [[2505.20800](#)].

[84] B. Shukla, P.P. Das, D. Dудal and S. Mahapatra, *Interplay between the Lyapunov exponents and phase transitions of charged AdS black holes*, *Phys. Rev. D* **110** (2024) 024068 [[2404.02095](#)].

[85] A. Kitaev, “Talks given at the Fundamental Physics Prize Symposium and KITP seminars.”

[86] S. Sachdev and J. Ye, *Gapless spin fluid ground state in a random, quantum Heisenberg magnet*, *Phys. Rev. Lett.* **70** (1993) 3339 [[cond-mat/9212030](#)].

[87] S.E. Aguilar-Gutierrez, Y. Fu, K. Pal and K. Parmentier, *Quasinormal modes and complexity in saddle-dominated $SU(N)$ spin systems*, *JHEP* **09** (2025) 039 [[2506.05458](#)].

[88] S. Chapman, S. Demulder, D.A. Galante, S.U. Sheorey and O. Shoval, *Krylov complexity and chaos in deformed Sachdev-Ye-Kitaev models*, *Phys. Rev. B* **111** (2025) 035141 [[2407.09604](#)].

[89] B. Bhattacharjee, X. Cao, P. Nandy and T. Pathak, *Krylov complexity in saddle-dominated scrambling*, *JHEP* **05** (2022) 174 [[2203.03534](#)].

[90] K.-B. Huh, H.-S. Jeong and J.F. Pedraza, *Spread complexity in saddle-dominated scrambling*, *JHEP* **05** (2024) 137 [[2312.12593](#)].

[91] J. Maldacena, D. Stanford and Z. Yang, *Conformal symmetry and its breaking in two dimensional Nearly Anti-de-Sitter space*, *PTEP* **2016** (2016) 12C104 [[1606.01857](#)].

[92] P. Saad, S.H. Shenker and D. Stanford, *A semiclassical ramp in SYK and in gravity*, [1806.06840](#).

[93] J. Maldacena and X.-L. Qi, *Eternal traversable wormhole*, [1804.00491](#).

[94] K. Jensen, *Chaos in AdS_2 Holography*, *Phys. Rev. Lett.* **117** (2016) 111601 [[1605.06098](#)].

[95] J. Polchinski and V. Rosenhaus, *The Spectrum in the Sachdev-Ye-Kitaev Model*, *JHEP* **04** (2016) 001 [[1601.06768](#)].

[96] D. Chowdhury, A. Georges, O. Parcollet and S. Sachdev, *Sachdev-Ye-Kitaev models and beyond: Window into non-Fermi liquids*, *Rev. Mod. Phys.* **94** (2022) 035004 [[2109.05037](#)].

[97] J.B. Hartle and S.W. Hawking, *Wave Function of the Universe*, *Phys. Rev. D* **28** (1983) 2960.

[98] W. Mück and Y. Yang, *Krylov complexity and orthogonal polynomials*, *Nucl. Phys. B* **984** (2022) 115948 [[2205.12815](#)].

[99] P. Caputa, J.M. Magan and D. Patramanis, *Geometry of Krylov complexity*, *Phys. Rev. Res.* **4** (2022) 013041 [[2109.03824](#)].

[100] J. Maldacena, S.H. Shenker and D. Stanford, *A bound on chaos*, *JHEP* **08** (2016) 106 [[1503.01409](#)].

[101] T. Anegawa and R. Watanabe, *Krylov complexity of fermion chain in double-scaled SYK and power spectrum perspective*, [2407.13293](#).

[102] M. Ambrosini, E. Rabinovici and J. Sonner, *Holography of K-complexity: Switchbacks and Shockwaves*, [2510.17975](#).

[103] M. Ambrosini, E. Rabinovici, A. Sánchez-Garrido, R. Shir and J. Sonner, *Operator K-complexity in DSSYK: Krylov complexity equals bulk length*, [2412.15318](#).

[104] D.A. Roberts, D. Stanford and A. Streicher, *Operator growth in the SYK model*, *JHEP* **06** (2018) 122 [[1802.02633](#)].

[105] X.-L. Qi and A. Streicher, *Quantum Epidemiology: Operator Growth, Thermal Effects, and SYK*, *JHEP* **08** (2019) 012 [[1810.11958](#)].

[106] A. Streicher, *SYK Correlators for All Energies*, *JHEP* **02** (2020) 048 [[1911.10171](#)].

[107] H.W. Lin, *The bulk Hilbert space of double scaled SYK*, *JHEP* **11** (2022) 060 [[2208.07032](#)].

[108] X.-L. Qi, E.J. Davis, A. Periwal and M. Schleier-Smith, *Measuring operator size growth in quantum quench experiments*, [1906.00524](#).

[109] H. Afshar, H.A. González, D. Grumiller and D. Vassilevich, *Flat space holography and the complex Sachdev-Ye-Kitaev model*, *Phys. Rev. D* **101** (2020) 086024 [[1911.05739](#)].

[110] H. Afshar and B. Oblak, *Flat JT gravity and the BMS-Schwarzian*, *JHEP* **11** (2022) 172 [[2112.14609](#)].

[111] P. Caputa, B. Chen, R.W. McDonald, J. Simón and B. Strittmatter, *Spread Complexity Rate as Proper Momentum*, [2410.23334](#).

[112] P. Caputa and G. Di Giulio, *Local quenches from a Krylov perspective*, *JHEP* **07** (2025) 164 [[2502.19485](#)].

[113] Z. Li and J. Tian, *The Holography of Spread Complexity: A Story of Observers*, [2506.13481](#).

[114] Z.-Y. Fan, *Momentum-Krylov complexity correspondence*, [2411.04492](#).

[115] P.-Z. He, *Revisit the relationship between spread complexity rate and radial momentum*, [2411.19172](#).

[116] S.E. Aguilar-Gutierrez, H.A. Camargo, V. Jahnke, K.-Y. Kim and M. Nishida, *Krylov operator complexity in holographic CFTs: Smeared boundary reconstruction and the dual proper radial momentum*, [2506.03273](#).

[117] D. Chakraborty and D. Rosa, *Revival Dynamics from Equilibrium States: Scars from Chords in SYK*, [2512.16836](#).

[118] Y. Jia and J.J.M. Verbaarschot, *Spectral Fluctuations in the Sachdev-Ye-Kitaev Model*, *JHEP* **07** (2020) 193 [[1912.11923](#)].

[119] W. Buijsman and Y.B. Lev, *Circular Rosenzweig-Porter random matrix ensemble*, *SciPost Phys.* **12** (2022) 082 [[2111.08031](#)].

[120] Y.-X. Wu, J.-F. Chen and H. Quan, *Ergodicity breaking and scaling relations for finite-time first-order phase transition*, *Physical Review Letters* **134** (2025) .

- [121] F. Barrows, E. Pelofske, P. Sathe, F. Caravelli and C. Nisoli, *Magnetic Memory and Hysteresis from Quantum Transitions: Theory and Experiments on Quantum Annealers*, [2507.18079](#).
- [122] F.J. Gómez-Ruiz, O.L. Acevedo, L. Quiroga, F.J. Rodríguez and N.F. Johnson, *Quantum Hysteresis in Coupled Light-Matter Systems*, *Entropy* **18** (2016) 319 [[1606.08823](#)].
- [123] T. Świsłocki, A. Zembrzuski, M. Matuszewski and E. Witkowska, *Dynamic hysteresis from bistability in an antiferromagnetic spinor condensate*, *Phys. Rev. A* **97** (2018) 033629 [[1803.03507](#)].
- [124] K.K. Kim, K.-Y. Kim, Y. Seo and S.-J. Sin, *Building magnetic hysteresis in holography*, *JHEP* **07** (2019) 158 [[1902.10929](#)].
- [125] M. Rangamani, M. Rozali and A. Vincart-Emard, *Dynamics of Holographic Entanglement Entropy Following a Local Quench*, *JHEP* **04** (2016) 069 [[1512.03478](#)].
- [126] T. Shimaji, T. Takayanagi and Z. Wei, *Holographic Quantum Circuits from Splitting/Joining Local Quenches*, *JHEP* **03** (2019) 165 [[1812.01176](#)].
- [127] J.L.F. Barbón, E. Rabinovici, R. Shir and R. Sinha, *On The Evolution Of Operator Complexity Beyond Scrambling*, *JHEP* **10** (2019) 264 [[1907.05393](#)].
- [128] V. Viswanath and G. Müller, *The recursion method: application to many body dynamics*, vol. 23, Springer Science & Business Media (1994).
- [129] B. Bhattacharjee, P. Nandy and T. Pathak, *Krylov complexity in large q and double-scaled SYK model*, *JHEP* **08** (2023) 099 [[2210.02474](#)].
- [130] M. Berkooz, N. Brukner, S.F. Ross and M. Watanabe, *Going beyond ER=EPR in the SYK model*, *JHEP* **08** (2022) 051 [[2202.11381](#)].
- [131] S. Forste, Y. Kruse and S. Natu, *Grand Canonical vs Canonical Krylov Complexity in Double-Scaled Complex SYK Model*, [2512.07715](#).
- [132] M. Miyaji, S. Mori and K. Okuyama, *Finite N bulk Hilbert space in ETH matrix model for double-scaled SYK. Null states, state-dependence and Krylov state complexity*, *JHEP* **08** (2025) 084 [[2505.13194](#)].
- [133] P. Nandy, *Tridiagonal Hamiltonians modeling the density of states of the double-scaled SYK model*, *JHEP* **01** (2025) 072 [[2410.07847](#)].